Energy Conversion and Management 276 (2023) 116556

Contents lists available at ScienceDirect

Energy Conversion and Management

journal homepage: www.elsevier.com/locate/enconman

Parametric and economic analysis of high-temperature cascade organic Rankine cycle with a biphenyl and diphenyl oxide mixture

Xiao Ren [a], Jing Li [b,*], Gang Pei [c], Pengcheng Li [d], Liang Gong [a]

[a] College of New Energy, China University of Petroleum (East China), Qingdao, China
[b] Research Center for Sustainable Energy Technologies, Energy and Environment Institute, University of Hull, Hull, UK
[c] Department of Thermal Science and Energy Engineering, University of Science and Technology of China, Hefei, China
[d] School of Automotive and Transportation Engineering, Hefei University of Technology, Hefei, China

ARTICLE INFO

Keywords:
Cascade organic Rankine cycle
High-temperature power generation
Biphenyl and diphenyl oxide mixture
Entropy generation
Economic assessment

ABSTRACT

High-temperature organic Rankine cycle (ORC) systems have the potential to improve the heat-to-power conversion efficiency and expand the temperature range for heat recovery, heat battery and solar power generation. Restricted by the critical temperature of the commonly used organic working fluids, the current ORC technology has a maximum working temperature of around 300 °C. This paper proposes a high-temperature cascade organic Rankine cycle (CORC) system using a biphenyl and diphenyl oxide (BDO) mixture as the top cycle fluid and conventional organic fluids for the bottom cycle. The BDO mixture has excellent heat stability over a wide operation condition from 12 °C to 400 °C in single-phase and binary-phase states. However, at present a detailed study on the ORC using the mixture is lacking. In this paper, a parametric analysis of the high-temperature CORC system is conducted. A mathematical model based on the equivalent hot side temperature is built to simulate the ORC efficiency. The thermodynamic and exergetic performances of the novel CORC system under different bottom ORC working fluids, mixing chamber temperatures, evaporation temperatures, and condensation temperatures are investigated. The results show the maximum thermal efficiency of the CORC system is 38.74 % and 40.26 % at top ORC evaporation temperatures of 360 °C and 400 °C. The largest exergy destruction takes place in the heat exchanger between the top and bottom ORCs. Besides, the heat regenerators have a significant impact on the thermodynamic performance and can elevate the CORC efficiency by about 4 %. The proposed system has a higher efficiency and a lower equipment cost than conventional steam Rankine cycle at 400 °C while eliminating the challenges of wet steam turbines.

1. Introduction

The organic Rankine Cycle (ORC) is considered one of the best technologies for heat to power conversion from low-temperature heat sources such as industrial waste heat [1,2], geothermal energy [3], solar energy [4], biomass energy [5] and ocean thermal energy [6]. The cascade organic Rankine cycle (CORC) can improve the heat-to-power conversion efficiency of the system and realize the step-by-step utilization of energy [7,8]. It is a good choice for medium and high temperature power generation [9]. The high-temperature CORC system can make better use of heat sources with the potential for efficiency promotion [10,11], and expands the operation temperature in the heat recovery and heat battery applications[12,13].

At present, commercially available ORC technologies have a maximum working temperature of around 300 °C, mainly because the evaporation temperature is limited by the critical temperature of the commonly used organic fluids. The ORC power generation efficiency is relatively low due to the temperature limitation. In the screening of ORC working fluids, hydrocarbons, siloxanes, refrigerants, and other pure organic working fluids have good performance in the utilization of medium- and low-temperature heat sources and are widely used as working fluids for ORC [14,15]. However, these working fluids have relatively low critical temperatures and cannot be used in high-temperature ORC systems above 300 °C. Fluids such as toluene and octamethyl cyclotetrasiloxane (D4) have high critical temperatures, but the operating temperature is limited to 318.60 °C and 313.35 °C [16]. Therefore, ORC and CORC are mainly studied and analyzed for medium- and low-temperature heat sources [17,18], and there are relatively few related studies on high-temperature heat sources, especially when the

* Corresponding author.
E-mail address: Jing.li@hull.ac.uk (J. Li).

https://doi.org/10.1016/j.enconman.2022.116556
Received 28 September 2022; Received in revised form 18 November 2022; Accepted 4 December 2022
Available online 14 December 2022

Nomenclature

A	area, m^2
Bo	boiling number
C	specific heat, $kJ{\cdot}kg^{-1}{\cdot}K^{-1}$/cost, $
D	diameter, m
f	factor/ Darcy resistance coefficient
G	mass flux, $kg/(m^2/s)$
H	enthalpy, kJ
h	enthalpy, kJ/kg
M	molar mass, g/mol
$\dot{m}$	mass flow rate, kg/s
p	pressure, kPa
Pr	Prandtl number
Q	heat, W
Re	Reynolds number
S	Entropy, kJ/K
s	Entropy, $kJ{\cdot}kg^{-1}{\cdot}K^{-1}$
T	temperature, K
t	operating time, h
U	heat transfer coefficient, $W/(m^{2}{\cdot}K)$
u	flow velocity, m/s
v	specific volume, m^3/kg
W	work, W
x	Quality

Greek letters

α	heat transfer coefficient, $W/(m^{2}{\cdot}K)$
δ	thickness, m
ε	machine efficiency
η	efficiency
λ	thermal conductivity, $W/(m{\cdot}K)$
ν	kinematic viscosity, m^2/s
ρ	density, kg/m^3

Subscripts

b	basic
bp	boiling point
bot	bottom ORC
c	critical condition
cool	cold side
CORC	cascade organic Rankine cycle
con	condensation
d	design condition
eva	evaporation
EHST	equivalent hot side temperature
g	generator
heat	hot side
HP	high-pressure
HX	heat exchanger
l	liquid
LP	low-pressure
M	material
m	log-mean
max	maximum
MC	mixing chamber
min	minimum
ORC	organic Rankine cycle
P	pump
p	pressure
pinch	pinch point
r	regenerator
s	isentropic
sl	saturated liquid
sv	saturated vapor
T	turbine/temperature
top	top ORC
tube	tube
v	vapor

heat source temperature exceeds 380 °C. In the high temperature range from 300 °C to 400 °C, waste heat recovery and solar thermal power generation call for more appropriate working fluids.

A biphenyl and diphenyl oxide (BDO) mixture is potentially suitable as the working fluid for high-temperature ORC systems. The mixture of biphenyl (26.5 %) and diphenyl oxide (73.5 %), as a well-known synthetic heat transfer fluid, is also known as the commercial name Therminol VP-1 or Dowtherm A [19]. The BDO mixture combines exceptional heat stability and low viscosity for efficient, dependable, uniform performance in a wide optimum use range from 12 °C to 400 °C [20]. It can be used in liquid, vapor, or binary phase states. At present, Therminol VP-1 has been widely used in the collectors for concentrated solar power generation, such as the parabolic trough solar collectors and linear Fresnel reflectors [21,22], and also in the hybrid concentrated photovoltaic/thermal system as a spectral beam filter [23].

Notably, the BDO mixture has significant potential in the ORC power generation application. Owing to the high vaporization temperature (about 400 °C), the mixture converts heat into power efficiently. The mixture is a dry organic fluid and can expand without droplets, leading to a high turbine efficiency. The expansion process decreases the fluid temperature, which enables the mixture to remain in a safe temperature range. Experimental results indicated the eutectic mixture had outstanding stability in a closed two-phase boiler loop with an outlet temperature of 371 °C during the 6367 h operation and there was no evident variation in the thermophysical properties (viscosity, refractive index, specific gravity, and freezing point) [24]. An ORC system utilizing the BDO mixture was described in the literature, which successfully operated over years [25]. More results showed the mixture did not suffer from decomposition after 5520 h in 316 stainless steel with repeated boiling/condensing cycles (one every 24 h) between 325 °C and 380 °C [26]. The mixture is capable to recover waste heat and drive the ORC at temperature up to 400 °C [27]. There is no technical barrier for the mixture to work as an ORC fluid [28].

The potential of the ORC using the BDO mixture in waste heat recovery has been outlined recently [29] and a brief simulation has been conducted [28]. However, literature on this topic is limited. It is still unclear how the efficiency of the ORC is affected by the heat source and heat sink temperatures and internal thermodynamic parameters. A detailed, parametric study is needed for a close view of its heat-to-power conversion performance and cost.

To fill the above knowledge gap, a parametric and economic analysis of the high-temperature CORC system using a biphenyl-diphenyl oxide mixture as the high temperature working fluid is conducted in this paper. A mathematical model based on the equivalent hot side temperature is established, which can make an in-depth performance prediction of the high-temperature CORC system. The influences of mixing chamber temperature, ORC working fluid, evaporation temperature, condensation temperature, and heat regenerator are investigated. A cost comparison with a conventional steam Rankine cycle (SRC) system is also made. The BDO mixture can overcome the evaporation temperature limitation by the critical temperature of common working fluids and avoid wet steam turbines, and thereby a high heat-to-power conversion efficiency is expected with a potential decrement in cost.

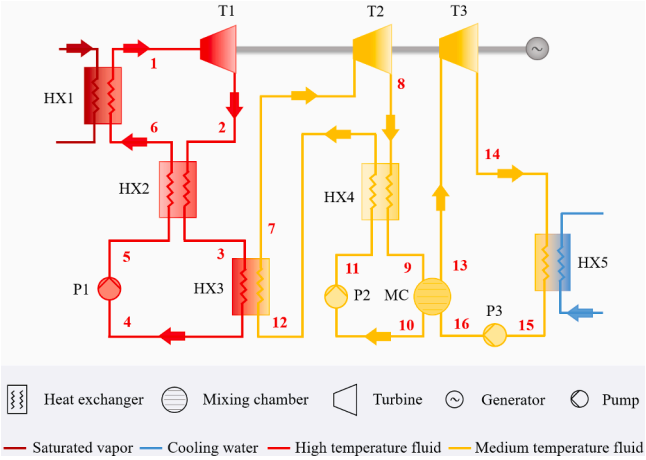

Fig. 1. Structure diagram of the high temperature CORC system.

Table 1
Typical properties of the BDO mixture.

Typical property	Value
Maximum bulk temperature	400 °C
Maximum film temperature	430 °C
Normal boiling point	257 °C
Crystallizing point	12 °C
Pseudocritical temperature	499 °C
Pseudocritical pressure	33.1 bar

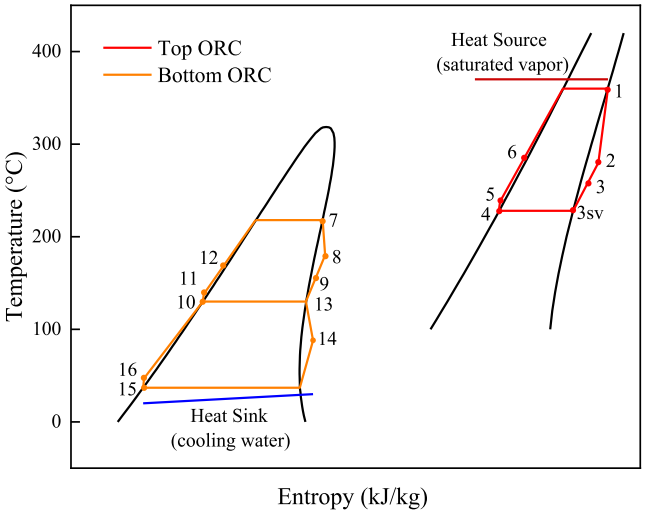

Fig. 2. *T-s* diagram of the high temperature CORC system.

2. System description

The schematic diagram of the proposed high-temperature CORC system is shown in Fig. 1, and the thermodynamic states are also marked with corresponding numbers. The high temperature CORC system consists of the top ORC and bottom ORC. In this system, the heat source can be solar energy, biomass energy or industrial waste heat, etc, and it is used to evaporate the working fluid in heat exchanger 1 (HX1). The BDO mixture is used for power conversion in the top ORC. The typical properties of the BDO mixture are shown in Table 1. The saturated vapor of the BDO mixture expands in the top ORC turbine (T1). Exhaust vapor at the superheated state is precooled in the heat regenerator HX2 and condensed into liquid and cooled down through the heat exchanger HX3. The BDO mixture from pump *P*1 is heated in the HX2 by the exhaust vapor from the top ORC turbine.

In the bottom ORC, organic fluids such as toluene, benzene, cyclohexane, and D4 can be used. Since the fluids of the top and bottom ORCs are different, the top ORC is coupled with the bottom high-pressure (HP) ORC unit through a heat exchanger HX3. The saturated vapor from HX3 flows into the bottom HP turbine to generate power, and a heat regenerator HX4 is used in the bottom ORC to improve the heat-to-power conversion efficiency. The superheated exhaust vapor is precooled in the HX4, condensed into liquid through the mixing chamber, and then flows into *P*2. Meanwhile, the saturated vapor from mixing chamber flows into the low-pressure turbine (LP turbine) to generate power and is condensed in HX5. The low-temperature liquid mixture is pressurized through *P*3 and sent to mixing chamber.

3. Mathematical model

The *T-s* diagram of the high-temperature CORC system is shown in Fig. 2, and the numbers indicate the thermodynamic states of top and bottom working fluids corresponding to the hallmarks of the high-temperature CORC system in Fig. 1. In the simulation, the heat and friction losses in the pipes and heat exchangers are disregarded, and the changes in kinetic and potential energy are ignored.

3.1. Top ORC

In the top ORC, the work generated by the top turbine is calculated by:

$$W_{T1} = \dot{m}_{top}(h_1 - h_2) = \dot{m}_{top}(h_1 - h_{2s})\varepsilon_T \tag{1}$$

where ε_T is the isentropic efficiency of the top and bottom ORC turbine; $\dot{m}_{top}$ is the mass flow rate of the top ORC (kg/s); h is the specific enthalpy value of each point (kJ/kg).

The heat balance in heat exchangers HX2 and HX3 is determined by:

$$\dot{m}_{top}(h_2 - h_3) = \dot{m}_{top}(h_6 - h_5) \tag{2}$$

$$\dot{m}_{top}(h_3 - h_4) = \dot{m}_{bot,HP}(h_7 - h_{12}) \tag{3}$$

The work required by the pump *P*1 is calculated by:

$$W_{P1} = \dot{m}_{top}(h_5 - h_4) = \dot{m}_{top}(h_{5s} - h_4) \Big/ \varepsilon_P \tag{4}$$

where ε_P is the isentropic efficiency of the working fluid pump.

The heat transferred to the working fluid in the evaporators of the top ORC is calculated by:

$$Q_{top} = \dot{m}_{top}(h_1 - h_6) \tag{5}$$

The thermophysical properties of BDO mixture cannot be acquired from REFPROP, but its saturation state parameters (pressure, enthalpy, density, and so on) can be obtained from a supplier [30]. Since the enthalpy of superheated vapor at the outlet of the HP turbine (h_2) cannot be derived directly, an ORC efficiency model based on the equivalent hot side temperature built by the authors [31] is used to calculate the efficiency, in which only the saturation parameters of the working fluid are required. The efficiency of top ORC with the most basic structure based on the equivalent hot side temperature is expressed as:

$$\eta_{ORC,b} = \left(1 - \frac{T_4}{T_{EHST}}\right) \cdot \frac{\varepsilon_T \varepsilon_g + v_4(p_1 - p_4) \Big/ \left(\varepsilon_p \int_1^{3sv} v_{sv} dp\right)}{1 + v_4(p_1 - p_4) \Big/ \left(\int_1^{3sv} v_{sv} dp\right)} \tag{6}$$

where v is the specific volume of each point (m^3/kg); ε_g is the generator's efficiency; T_{EHST} is the equivalent hot side temperature (K) and calculated by:

$$T_{EHST} = \frac{h_1 - h_4 - v_4(p_1 - p_4)}{s_1 - s_4} \tag{7}$$

Table 2
Saturation state parameters of the BDO mixture.

T (°C)	p (kPa)	h_{sl} (kJ·kg^{-1})	ρ_{sl} (kg·m^{-3})	$C_{p,sl}$ (kJ·kg^{-1}·K^{-1})	s_{sl} (kJ·kg^{-1}·K^{-1})	h_{sv} (kJ·kg^{-1})	ρ_{sv} (kg·m^{-3})	$C_{p,sv}$ (kJ·kg^{-1}·K^{-1})	s_{sv} (kJ·kg^{-1}·K^{-1})
200	23.9	336.5	913	2.05	3.453	659.4	1.02	1.57	4.136
220	41.5	378.0	895	2.10	3.539	691.0	1.71	1.63	4.174
240	68.4	420.5	877	2.15	3.623	723.5	2.72	1.68	4.214
260	108	464.1	857	2.21	3.707	756.9	4.17	1.74	4.256
280	163	508.8	838	2.26	3.789	791.0	6.17	1.79	4.299
300	239	554.6	817	2.31	3.870	825.8	8.86	1.84	4.343
320	340	601.4	796	2.37	3.950	861.1	12.4	1.90	4.388
340	470	649.3	773	2.43	4.029	896.9	17.0	1.95	4.433
360	635	698.4	749	2.49	4.108	933.1	22.9	2.00	4.478
380	840	748.7	722	2.55	4.186	969.5	30.5	2.05	4.532
400	1090	800.5	694	2.63	4.263	1005.8	40.1	2.11	4.568

Table 3
Thermophysical parameters of the bottom ORC fluids.

	T_c (°C)	p_c (kPa)	T_{bp} (°C)	M (g/mol)
Toluene	318.60	4126	110.60	92.14
D4	313.35	1332	175.35	296.62
Benzene	288.87	4894	80.07	78.11
Cyclohexane	280.49	4075	80.74	84.16

Table 4
Specific parameters of high-temperature CORC system in the simulation.

Parameter	Value
Rated output power of CORC system, W_{CORC}	10 MW$_e$
ORC turbine isentropic efficiency, ε_T	85 %
Pump isentropic efficiency ($P1$, $P2$, and $P3$), ε_P	80 %
Generator efficiency, ε_g	95 %
Regenerator efficiency (HX2 and HX4), ε_r	70 %
Minimum temperature difference, ΔT_{min}	10 °C

Meanwhile, the efficiency of top ORC with the most basic structure can be expressed as:

$$\eta_{ORC,b} = \frac{(h_1 - h_2)\varepsilon_g - (h_5 - h_4)}{h_1 - h_5} \tag{8}$$

Therefore, according to Eq. (6) and Eq. (8), h_2 can be deduced.

Most ORC fluids in a liquid state are not compressible and most of the heat is taken out by the condensation process [31], thus the h_{5s} can be calculated by:

$$h_{5s} \approx h_4 + v_4(p_{5s} - p_4) \tag{9}$$

Besides, the entropy of the BDO mixture is not provided. Since entropy is a state parameter, the selection of reference points does not affect the change of entropy. Therefore, in this paper, the entropy of saturated liquid at 373.15 K (100 °C) is set to 3 kJ/(kg·K), and then the entropy of saturated state at different temperatures can be derived from the following thermodynamic relation:

$$dh = Tds + vdp \tag{10}$$

It is found that the values between superheated vapor and saturated vapor with the same enthalpy are very close under the premise of low superheat [32]. Therefore, the specific heat at a constant pressure of point 2 is approximately equal to that of saturated steam with the same enthalpy. The BDO mixture after expansion generally has a pressure lower than 100 kPa and a temperature higher than 250 °C. Assuming that the enthalpy in the process from point 2 to point 3sv is a function of temperature, the temperature at point 2 can be approximately calculated by:

$$\delta h = c_p dT$$

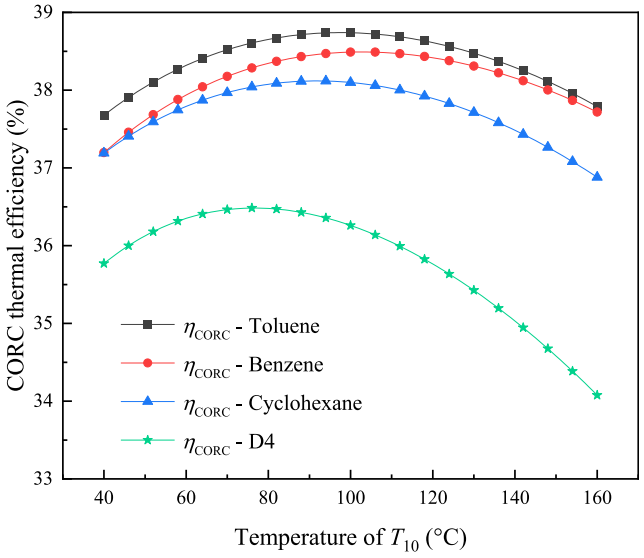

Fig. 3. Variation of the CORC thermal efficiency of the CORC system.

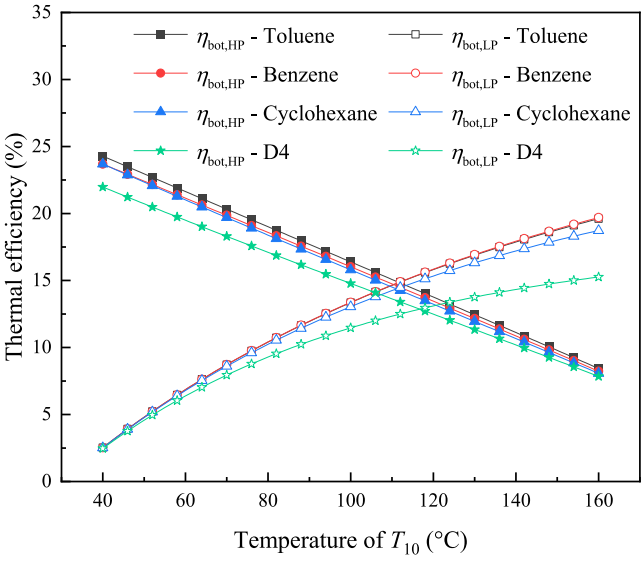

Fig. 4. Variation of the bottom ORC thermal efficiency of the CORC system.

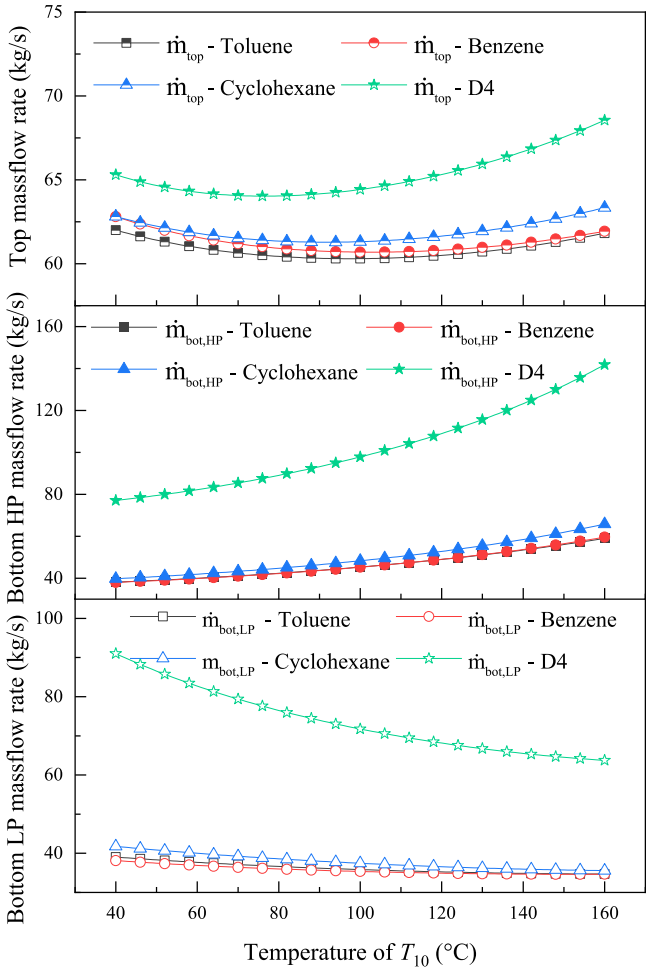

Fig. 5. Variation of the mass flow rate of the top, bottom HP, and bottom LP ORCs.

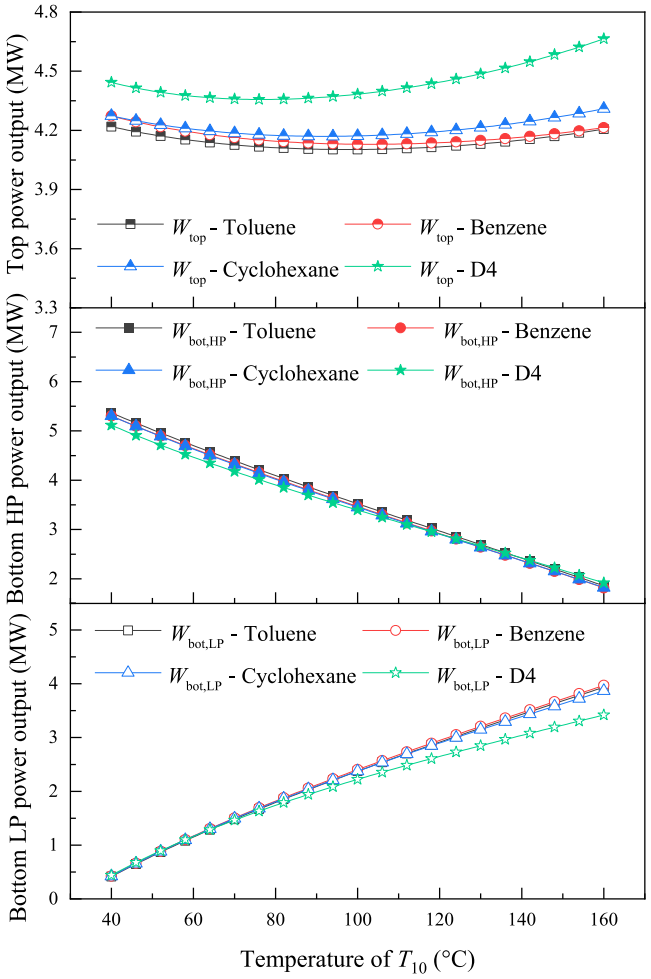

Fig. 6. Variation of the power output of the top, bottom HP, and bottom LP ORCs.

$$T_2 = T_{3sv} + \frac{h_2 - h_{3sv}}{\overline{c_p}}$$

where $\overline{c_p}$ is the average specific heat at constant pressure at points 2 and 3sv.

Integrating the points 2 to 2 s ($dp = 0$) according to the thermodynamic Eq. (10), the entropy of point 2 can be obtained by:

$$s_2 = s_{2s} + \frac{h_2 - h_{2s}}{\overline{T}}$$

where $\overline{T}$ is the average temperature at points 2 and 2 s, and the enthalpy of point 2 s is calculated by:

$$h_{2s} = h_1 - \frac{h_1 - h_2}{\varepsilon_T}$$

3.2. Bottom ORC

The work generated by the bottom HP turbine in the bottom ORC is determined by:

$$W_{T2} = \dot{m}_{bot,HP}(h_7 - h_8) = \dot{m}_{bot,HP}(h_7 - h_{8s})\varepsilon_T \quad (15)$$

The work required by the pumps *P*2 is calculated by:

$$W_{P2} = \dot{m}_{bot,HP}(h_{11} - h_{10}) = \dot{m}_{bot,HP}(h_{11s} - h_{10}) \Big/ \varepsilon_P \quad (16)$$

In the bottom ORC, the heat transferred to the working fluid in the evaporator is calculated by:

$$Q_{bot,HP} = \dot{m}_{bot,HP}(h_7 - h_{12}) \quad (17)$$

In the bottom LP ORC, the work generated by the bottom LP turbine can be calculated by:

$$W_{T3} = \dot{m}_{bot,LP}(h_{14} - h_{13}) = \dot{m}_{bot,LP}(h_{14} - h_{13s})\varepsilon_T \quad (18)$$

The work required by the pumps *P*3 is determined by:

$$W_{P3} = \dot{m}_{bot,LP}(h_{16} - h_{15}) = \dot{m}_{bot,LP}(h_{16s} - h_{15}) \Big/ \varepsilon_P \quad (19)$$

The heat transferred to the working fluid flowing into the bottom LP turbine is calculated:

$$Q_{bot,LP} = \dot{m}_{bot,LP}(h_{13} - h_{16}) \quad (20)$$

3.3. Performance evaluation

The work of the top, bottom HP, and bottom LP ORCs can be expressed as:

$$W_{top} = W_{T1}\varepsilon_g - W_{P1} \quad (21)$$

$$W_{bot,HP} = W_{T2}\varepsilon_g - W_{P2} \quad (22)$$

$$W_{bot,LP} = W_{T3}\varepsilon_g - W_{P3} \quad (23)$$

The work of the CORC is calculated by:

Table 5
Parameters of the high-temperature CORC system at maximum CORC efficiency.

	T_{10} (°C)	W_{top} (MW)	$W_{bot,HP}$ (MW)	$W_{bot,LP}$ (MW)	η_{top} (%)	$\eta_{bot,HP}$ (%)	$\eta_{bot,LP}$ (%)	$\eta_{CORC,max}$ (%)
Toluene	98	4.10	3.58	2.32	15.89	16.65	13.08	38.74
Benzene	103	4.13	3.38	2.49	15.89	15.64	13.77	38.49
Cyclohexane	92	4.17	3.68	2.15	15.89	16.83	11.99	38.12
D4	77	4.36	3.98	1.66	15.89	17.46	8.91	36.48

Table 6
Parameters distribution of the CORC system using toluene at maximum CORC efficiency.

	T (°C)	h (kJ/kg)	p (kPa)	s (kJ·kg^{-1}·K^{-1})	ṁ(kg/s)
1	360	933.06	635.12	4.48	60.30
2	316.38	860.57	50.68	4.50	60.30
3	256.17	751.48	50.68	4.28	60.30
4	228	395.07	50.68	3.57	60.30
5	228.54	395.89	635.12	3.57	60.30
6	278.36	504.98	635.12	3.78	60.30
7	218	511.52	1020.04	1.10	44.98
8	151.75	426.19	69.85	1.13	44.98
9	115.11	369.03	69.85	0.99	44.98
10	98	−24.95	69.85	−0.07	44.98
11	98.44	−23.45	1020.04	−0.07	44.98
12	126.90	33.71	1020.04	0.08	44.98
13	98	343.89	69.85	0.93	35.91
14	43.27	275.83	4.89	0.97	35.91
15	30	−149.69	4.89	−0.44	35.91
16	30.03	−149.60	69.85	−0.44	35.91

$$W_{CORC} = (W_{T1} + W_{T2} + W_{T3})\varepsilon_g - W_{P1} - W_{P2} - W_{P3} \tag{24}$$

The thermal efficiencies of the top ORC, bottom HP ORC, bottom LP ORC, and CORC are expressed as:

$$\eta_{top} = W_{top}/Q_{top} \tag{25}$$

$$\eta_{bot,HP} = W_{bot,HP}/Q_{bot,HP} \tag{26}$$

$$\eta_{bot,LP} = W_{bot,LP}/Q_{bot,LP} \tag{27}$$

$$\eta_{CORC} = W_{CORC}/Q_{top} \tag{28}$$

3.4. Entropy generation

The entropy generation of various components such as the ORC turbines, heat exchangers, and pumps represents the thermodynamic irreversibility of the proposed high-temperature CORC system. The entropy generation of the top turbine, bottom HP turbine, and bottom LP turbine is expressed as:

$$\Delta S_{T1} = S_2 - S_1 \tag{29}$$

$$\Delta S_{T2} = S_8 - S_7 \tag{30}$$

$$\Delta S_{T3} = S_{14} - S_{13} \tag{31}$$

The entropy generation of the heat exchanger HX1, HX2, HX3, HX4, HX5, and mixing chamber is determined by:

$$\Delta S_{HX1} = S_1 - S_6 - (H_1 - H_6)/T_{heat} \tag{32}$$

$$\Delta S_{HX2} = S_6 - S_5 + S_3 - S_2 \tag{33}$$

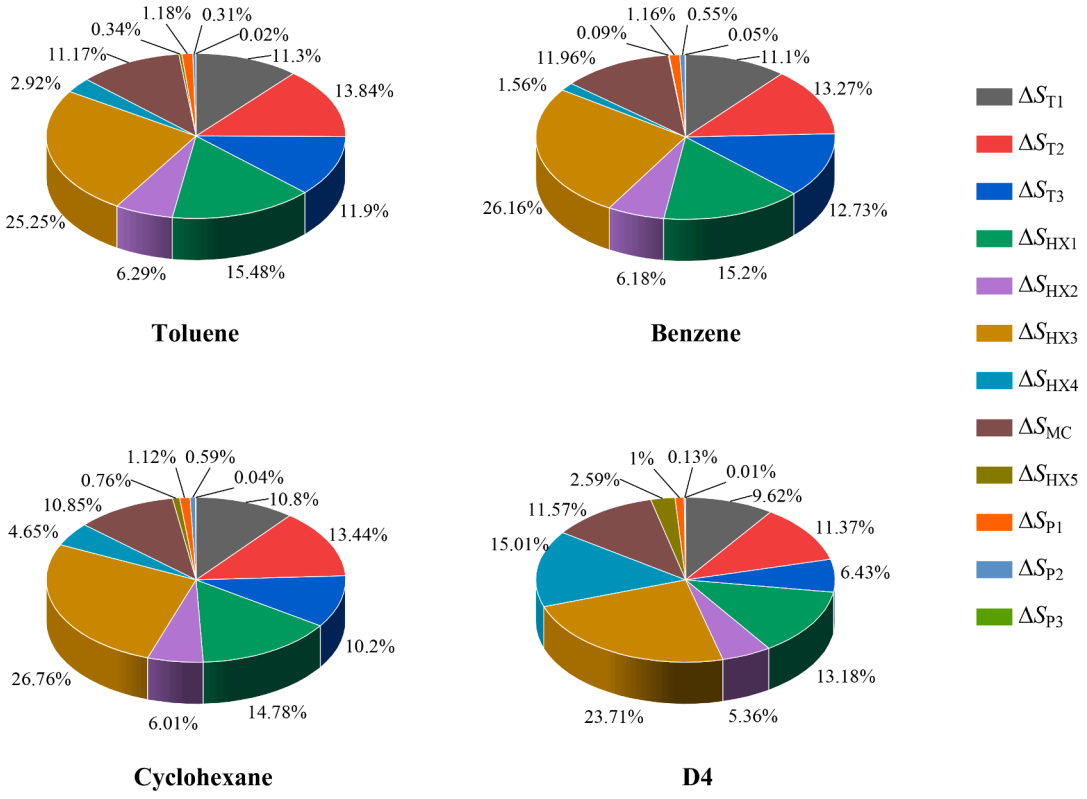

Fig. 7. Entropy generation at maximum CORC efficiency.

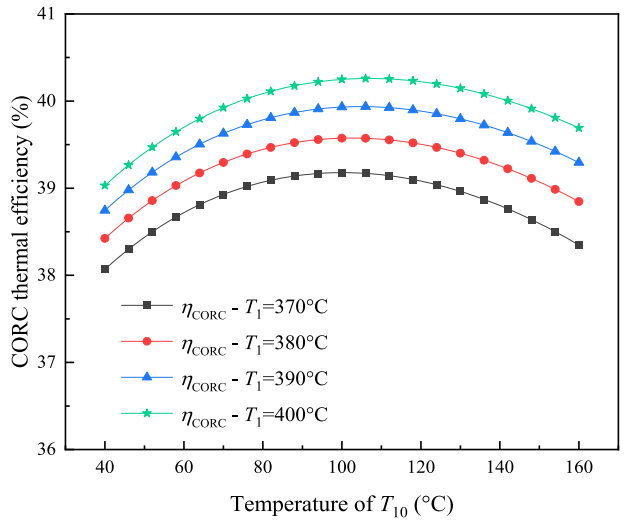

Fig. 8. Variation of the thermal efficiency of the CORC system at different evaporation temperatures.

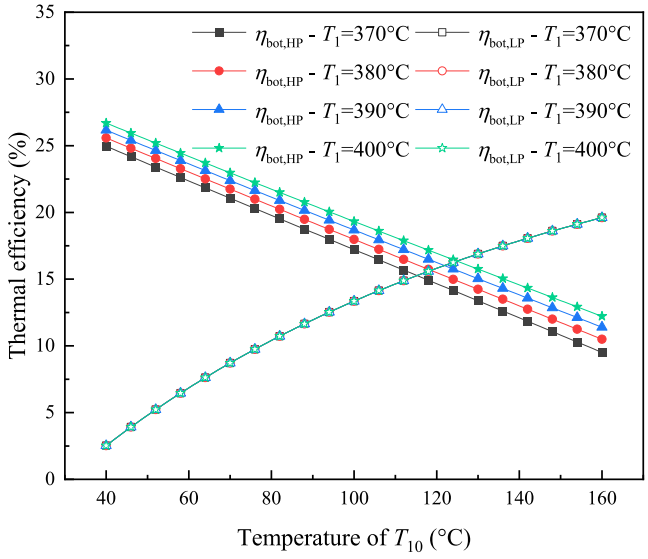

Fig. 9. Variation of the bottom ORC thermal efficiency at different evaporation temperatures.

$$\Delta S_{HX3} = S_4 - S_3 + S_7 - S_{12} \tag{34}$$

$$\Delta S_{HX4} = S_{12} - S_{11} + S_9 - S_8 \tag{35}$$

$$\Delta S_{HX5} = S_{15} - S_{14} - (H_{15} - H_{14})/T_{cool} \tag{36}$$

$$\Delta S_{MC} = S_{10} - S_9 + S_{13} - S_{16} \tag{37}$$

The entropy generation of the pump *P*1, *P*2, and *P*3 is calculated by:

$$\Delta S_{P1} = S_5 - S_4 \tag{38}$$

$$\Delta S_{P2} = S_{11} - S_{10} \tag{39}$$

$$\Delta S_{P3} = S_{16} - S_{15} \tag{40}$$

3.5. Economic assessment

In the economic analysis, the costs of the CORC system and a conventional SRC system are assessed at the same power output. The

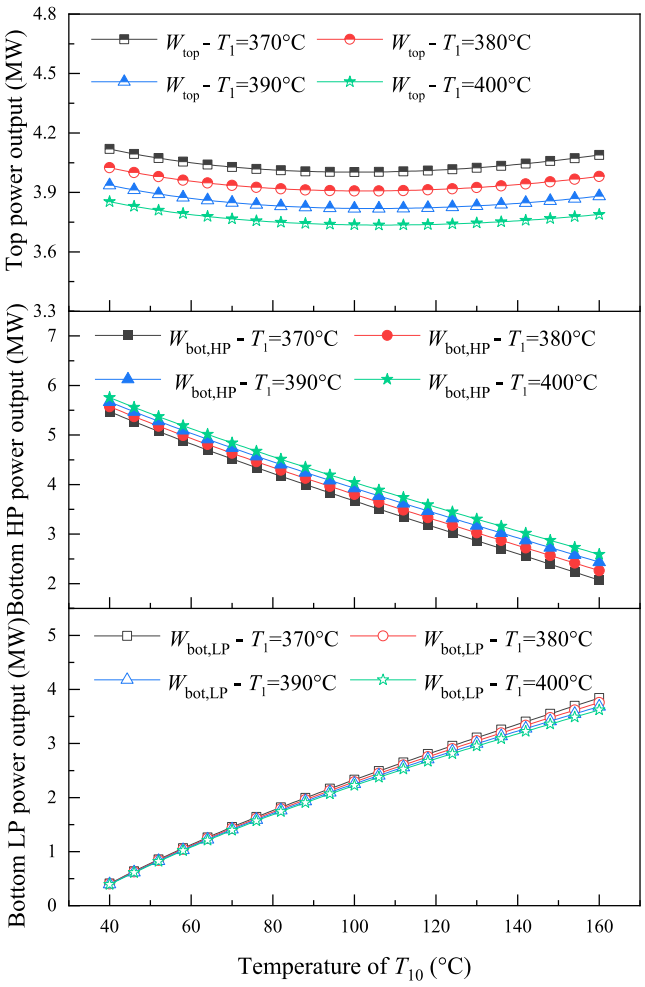

Fig. 10. Variation of the power output of the top, bottom HP, and bottom LP ORCs at different evaporation temperatures.

equipment costs of turbine [33], generator [34], pump [35], and heat exchanger [35] are defined as:

$$C_T = 6000 W_T^{0.7} \tag{41}$$

$$C_g = 60 W_g^{0.95} \tag{42}$$

$$C_P = 9.84 \times 10^3 \left(\frac{W_P}{4}\right)^{0.55} f_M f_P f_T \tag{43}$$

$$C_{HX} = 3.28 \times 10^4 \left(\frac{A_{HX}}{80}\right)^{0.68} f_M f_P f_T \tag{44}$$

where W_T, W_g and W_P are the consumed or generated work of the turbine, generator, and pump (kW); A_{HX} is heat transfer surface of the heat exchanger (m^2). HTRI software, an advanced thermal process design and simulation tool in the industry, is used to estimate the heat transfer area of the heat exchangers. The details on the heat transfer area calculation are given in Appendix; f_M, f_p, and f_T are the material factor, pressure factor, and temperature factor of the construction capital cost.

As the mixing chamber has a significantly lower cost than other components, its investment cost is ignored [36]. The total cost of the system is expressed by:

$$C_{CORC} = C_{HX} + C_P + C_T + C_g \tag{45}$$

Table 7
Parameters at the maximum CORC efficiency at different evaporation temperatures.

T_1 (°C)	T_4 (°C)	T_{10} (°C)	W_{top} (MW)	$W_{bot,HP}$ (MW)	$W_{bot,LP}$ (MW)	η_{top} (%)	$\eta_{bot,HP}$ (%)	$\eta_{bot,LP}$ (%)	$\eta_{CORC,max}$ (%)
360	228	98	4.10	3.58	2.32	15.89	16.65	13.08	38.74
365	233	99	4.05	3.63	2.32	15.79	16.	12.81	38.96
370	238	100	4.00	3.67	2.33	15.68	17.22	13.35	39.18
375	243	101	3.95	3.71	2.34	15.57	17.48	13.49	39.38
380	248	103	3.91	3.72	2.37	15.46	17.60	13.75	39.58
385	253	104	3.86	3.76	2.38	15.36	17.84	13.88	39.76
390	258	105	3.82	3.80	2.38	15.25	18.07	14.01	39.94
395	263	106	3.78	3.83	2.39	15.14	18.28	14.14	40.10
400	268	107	3.74	3.86	2.40	15.04	18.49	14.27	40.26

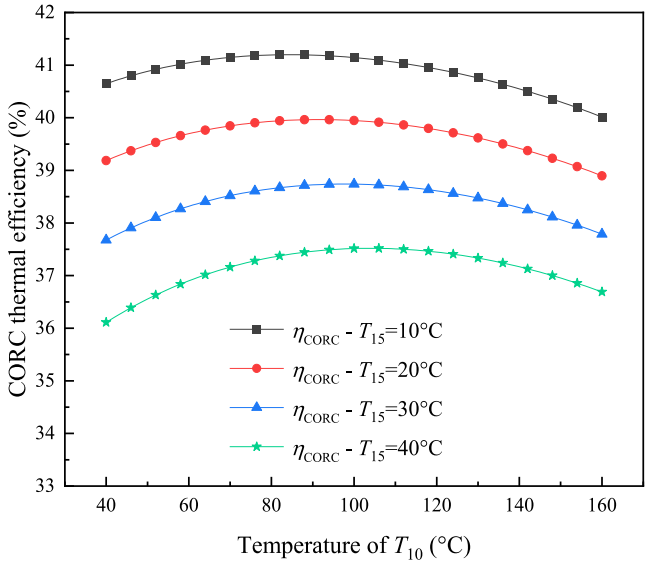

Fig. 11. Variation of the thermal efficiency of the CORC system at different condensation temperatures.

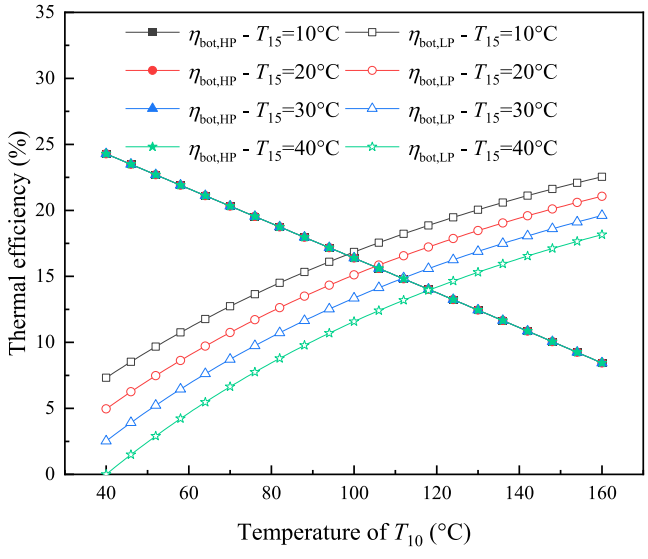

Fig. 12. Variation of the bottom ORC thermal efficiency at different condensation temperatures.

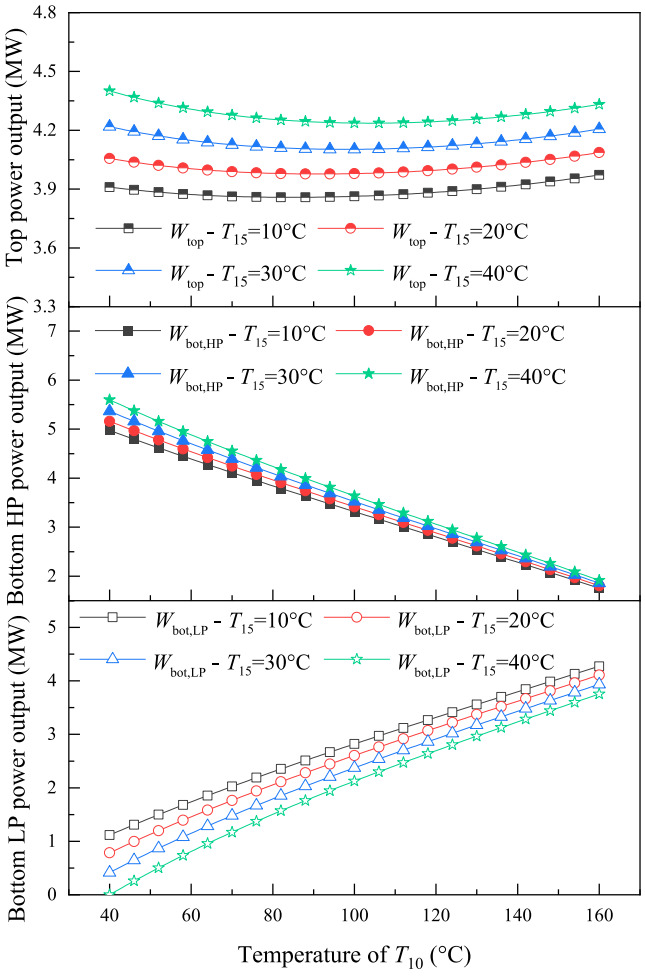

Fig. 13. Variation of the power output of the top, bottom HP, and bottom LP ORCs at different condensation temperatures.

Table 8
Parameters at the maximum CORC efficiency at different condensation temperatures.

T_{15} (°C)	T_{10} (°C)	W_{top} (MW)	$W_{bot,HP}$ (MW)	$W_{bot,LP}$ (MW)	η_{top} (%)	$\eta_{bot,HP}$ (%)	$\eta_{bot,LP}$ (%)	$\eta_{CORC,max}$ (%)
10	84	3.86	3.73	2.41	15.89	18.49	14.79	41.20
15	88	3.92	6.68	2.40	15.89	17.96	14.42	40.58
20	91	3.98	3.66	2.36	15.89	17.57	13.92	39.97
25	95	4.04	3.61	2.35	15.89	17.04	13.57	39.35
30	98	4.10	3.58	2.32	15.89	16.65	13.08	38.74
35	101	4.17	3.55	2.28	15.89	16.26	12.61	38.13
40	104	4.24	3.52	2.24	15.89	15.87	12.14	37.52

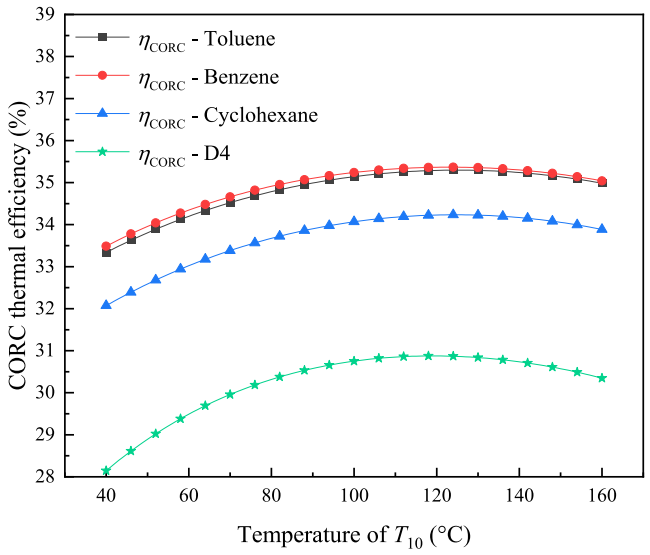

Fig. 14. Variation of the thermal efficiency of the CORC system without any regenerators.

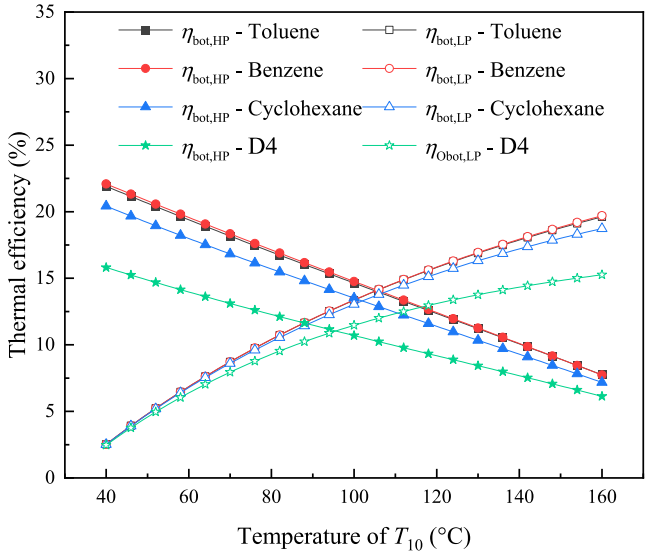

Fig. 15. Variation of the bottom ORC thermal efficiency without any regenerators.

4. Results and discussion

In the top ORC, the BDO mixture is used as the working fluid. The available saturation state parameters by the supplier and the calculation results of its entropy from 200 °C to 400 °C are shown in Table 2. In the calculation, the temperature interval is 1 °C and Table 2 summarizes some results. In the bottom ORC, four widely investigated and used fluids such as toluene[37,38], D4 [39,40], benzene[41,42], and cyclohexane [43,44] with critical temperatures of 318.60 °C, 313.35 °C, 288.87 °C, and 280.49 °C are selected. Thermophysical parameters of the toluene, D4, benzene, and cyclohexane are shown in Table 3. The specific parameters of the high-temperature CORC system in the simulation are shown in Table 4. The rated output power of the high temperature CORC system is 10 MW_e. The isentropic efficiency of the ORC turbines and pumps is 85 % and 80 %, respectively, and the regenerator efficiency of HX2 and HX4 is set to 70 %.

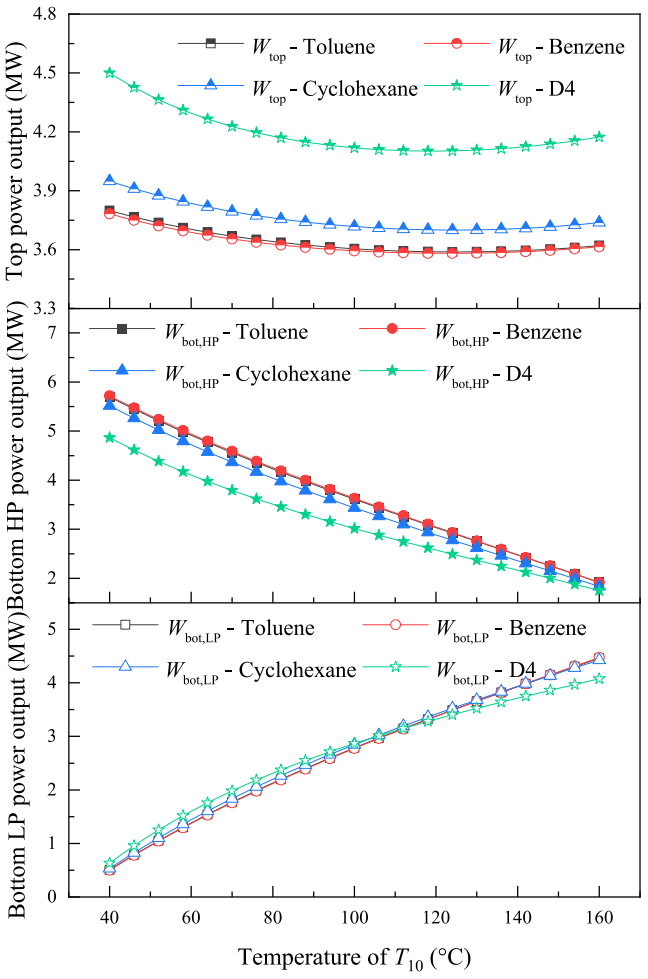

Fig. 16. Variation of the power output of the top, bottom HP, and bottom LP ORCs without any regenerators.

4.1. Parametric analysis of the CORC with regenerators

The influences of the mixing chamber temperature, top ORC evaporation temperature, and bottom ORC condensation temperature on the performance of the proposed system with the regenerators are investigated. The system design is illustrated in Fig. 1. The influences on the system without the regenerators will be examined in Section 4.2.

4.1.1. Influence of mixing chamber temperature

In this section, the CORC evaporation temperature and condensation temperature are set to 360 °C and 30 °C. The temperature at the outlet of the HX3 in the top ORC is set to 228 °C for the following reasons. First, the pressure of point 4 at 228 °C is higher than 50 kPa. This avoids a high vacuum of the regenerator HX2 and thus reduces the technical requirement and cost of the regenerator. Second, a high efficiency is achievable for the top ORC with an acceptable accuracy of the ORC model based on the equivalent hot side temperature. A lower degree of superheat at point 2 generally offers more accurate results.

Variations of the heat-to-power efficiency of the high-temperature CORC with the mixing chamber temperature (T_{10} or T_{13}) are given in Fig. 3. At different temperatures of T_{10}, the CORC thermal efficiencies with four different organic fluids in the bottom ORCs all present a shape similar to a parabola facing downward. The maximum CORC thermal efficiency for the bottom ORC fluids of toluene, benzene, cyclohexane, and D4 is 38.74 %, 38.49 %, 38.12 %, and 36.48 % when the mixing chamber temperature T_{10} is 98 °C, 103 °C, 92 °C, and 77 °C, respectively. Among them, the overall CORC thermal efficiency for toluene is

Table 9
Parameters at the maximum CORC efficiency without any regenerators.

	T_{10} (°C)	W_{top} (MW)	$W_{bot,HP}$ (MW)	$W_{bot,LP}$ (MW)	η_{top} (%)	$\eta_{bot,HP}$ (%)	$\eta_{bot,LP}$ (%)	$\eta_{CORC,max}$ (%)
Toluene	125	3.59	2.89	3.52	12.67	11.78	16.36	35.30
Benzene	123	3.58	2.96	3.46	12.67	12.08	16.18	35.37
Cyclohexane	124	3.70	2.78	3.52	12.67	10.97	15.74	34.23
D4	119	4.10	2.60	3.30	12.67	9.25	13.03	30.88

Table 10
Parameters distribution at the maximum CORC efficiency of the CORC system without any regenerators.

	T (°C)	h (kJ/kg)	p (kPa)	s (kJ·kg^{-1}·K^{-1})	ṁ(kg/s)
1	360	933.06	635.12	4.48	52.74
2	316.38	860.57	50.68	4.50	52.74
3	/	/	/	/	/
4	228	395.07	50.68	3.57	52.74
5	228.54	395.89	635.12	3.57	52.74
6	/	/	/	/	/
7	218	511.52	1020.04	1.10	51.06
8	168.07	450.38	149.95	1.12	51.06
9	/	/	/	/	/
10	125	29.28	149.95	0.07	51.06
11	125.44	30.70	1020.04	0.08	51.06
12	/	/	/	/	/
13	125	380.31	149.95	0.96	40.59
14	53.9	288.83	4.89	1.01	40.59
15	30	−149.69	4.89	−0.44	40.59
16	30.06	−149.48	149.95	−0.44	40.59

the highest, probably attributed to the highest critical temperature and latent heat for evaporation. The overall CORC thermal efficiency for D4 is the lowest and decreases significantly from the maximum point with the increase in T_{10}. The results show that the ORC working fluids perform a significant effect on the thermodynamic properties of the high-temperature CORC system. At given evaporation and condensation temperatures of 360 °C and 228 °C, the top ORC thermal efficiency remains at 15.89 %. As shown in Fig. 4, the thermal efficiencies of the bottom HP and LP ORCs using the four organic fluids show an opposite trend as the mixing chamber temperature T_{10} increases. The higher the mixing chamber temperature, the lower the bottom HP ORC thermal efficiency and the higher the bottom LP ORC thermal efficiency. Taking toluene as an example, when the mixing chamber temperature is 40 °C, 80 °C, 120 °C, and 160 °C, the bottom HP ORC thermal efficiency is 26.16 %, 19.01 %, 13.77 %, and 4.43 %, and the bottom LP ORC thermal efficiency is 2.53 %, 10.41 %, 15.81 %, and 19.61 %, respectively. Fig. 4 also indicates the variations of power outputs of the HP and LP ORC turbines. A higher bottom HP ORC efficiency is accompanied by a higher HP turbine output.

Variation of the mass flow rate of the top and bottom ORCs with the mixing chamber temperature T_{10} is shown in Fig. 5. As the mixing chamber temperature T_{10} increases, the mass flow rate of the top ORC decreases first and then increases. The reason is that the power output of the CORC is fixed at 10 MW and the mass flow rate is correlated to the efficiency. A higher CORC efficiency results in less heat transfer in the evaporator HX1 and vice versa. Given the inlet and outlet temperature/pressure at HX1, the mass flow rate of the top ORC is proportional to the heat transfer in HX1. The mass flow rates through the bottom HP and LP turbines vary differently. The former gradually increases and the latter decreases. As T_{10} rises, the enthalpy difference between points 7 and 12

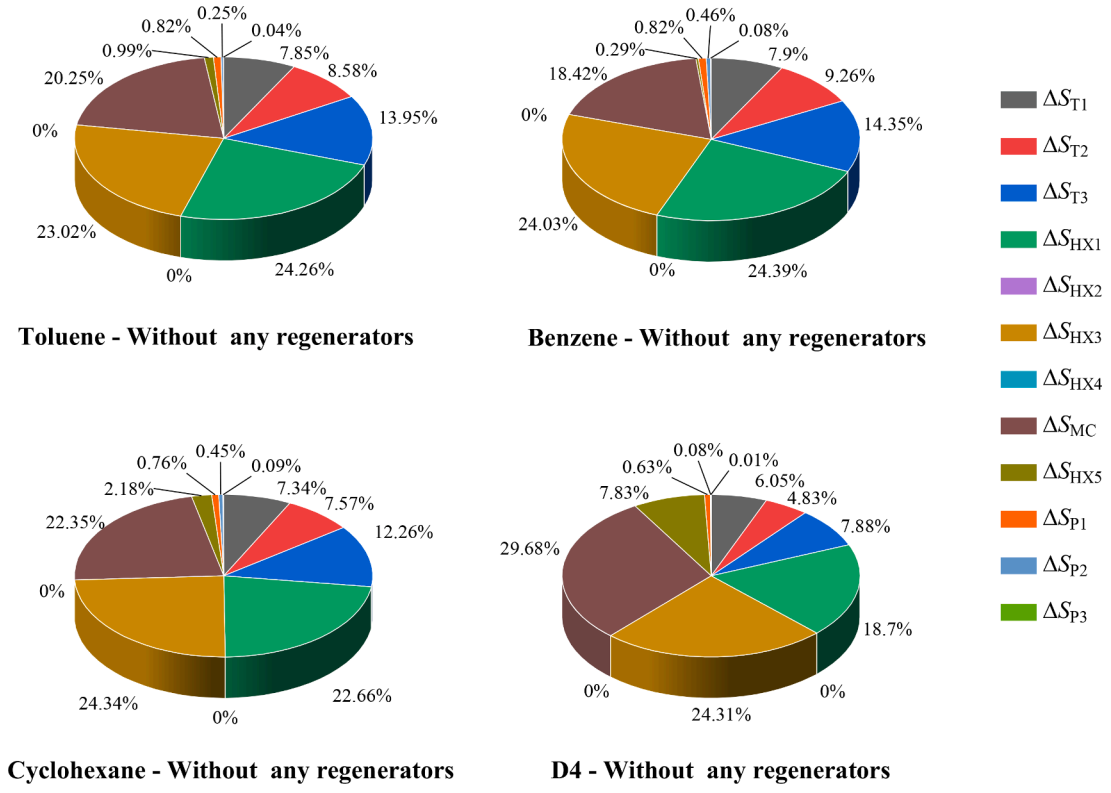

Fig. 17. Entropy generation at maximum CORC efficiency without any regenerators.

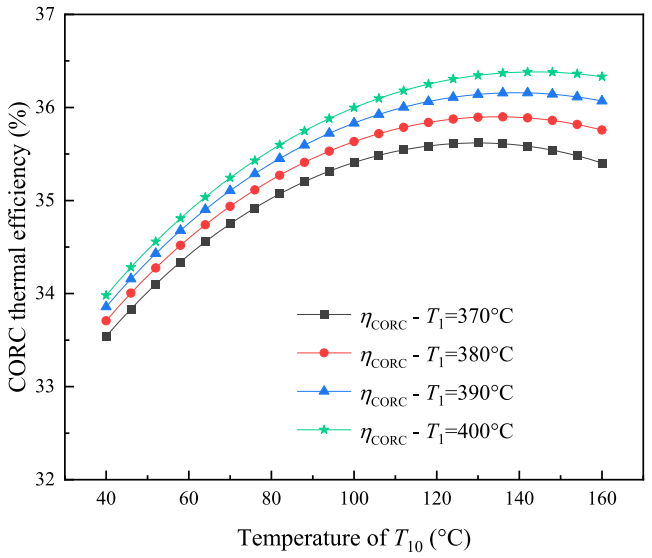

Fig. 18. Variation of the thermal efficiency of the CORC system without any regenerators at different evaporation temperatures.

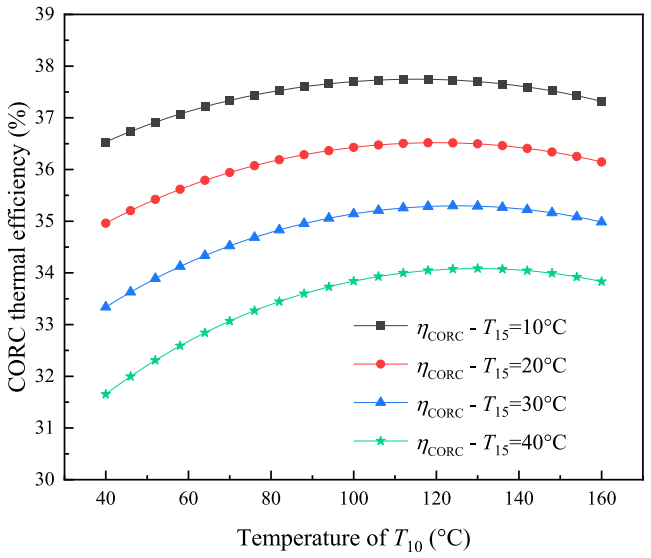

Fig. 19. Variation of the thermal efficiency of the CORC system without any regenerators at different condensation temperatures.

decreases, and a larger flow rate in HX3 is needed. On the contrary, the enthalpy difference between points 13 and 16 increases. The mass flow rates for the top and bottom ORCs using D4 are significantly higher than that using toluene, benzene, and cyclohexane.

As shown in Fig. 6, variations of the power outputs of the top turbine, bottom HP turbine, and bottom LP turbine are displayed. With an increasing mixing chamber temperature T_{10}, the power output of top ORC decreases first and then rises, while the outputs of bottom HP and LP ORCs increase and decrease gradually, respectively. When the working fluid of the bottom ORC is toluene, benzene, cyclohexane, and D4, the minimum output of the top ORC is 4.13 MW, 4.14 MW, 4.21 MW, and 4.47 MW. Similarly, taking toluene as an example, when the mixing chamber temperature is 40 °C, 80 °C, 120 °C, and 160 °C, the power output of bottom HP ORC is 5.37 MW, 4.09 MW, 2.97 MW, and 1.86 MW, and it is 0.41 MW, 1.80 MW, 2.91 MW, and 3.93 MW for the bottom LP ORC.

Details on the optimum mixing chamber temperature, power output, and thermal efficiency of the top, bottom HP, and bottom LP ORCs under the maximum CORC thermal efficiency for different working fluids are presented in Table 5. Moreover, the parameter distribution (temperature, enthalpy, pressure, entropy, and mass flowrate) of each point in the high-temperature CORC system using toluene at maximum CORC efficiency is given in Table 6.

The entropy generation of each equipment in the high-temperature CORC systems under the maximum CORC efficiency conditions is shown in Fig. 7. The entropy generation represents the exergy thermodynamic irreversibility of the CORC system. For all the four bottom ORC fluids, the entropy generation in the heat exchanger HX3 is the highest, accounting for about 1/4 of the total entropy production of the system.

Table 12
Parameters of the CORC without any generators at different condensation temperatures.

T_{15} (°C)	T_{10} (°C)	W_{top} (MW)	$W_{bot,HP}$ (MW)	$W_{bot,LP}$ (MW)	η_{top} (%)	$\eta_{bot,HP}$ (%)	$\eta_{bot,LP}$ (%)	$\eta_{CORC,max}$ (%)
10	115	3.35	2.97	3.68	12.67	12.92	18.54	38.75
15	118	3.41	2.94	3.65	12.67	12.58	18.04	37.13
20	120	3.47	2.93	3.60	12.67	12.35	17.44	36.52
25	123	3.53	2.90	3.57	12.67	12.01	16.95	35.91
30	125	3.59	2.89	3.52	12.67	11.78	16.36	35.30
35	128	3.65	2.86	3.49	12.67	11.44	15.89	34.69
40	130	3.72	2.85	3.43	12.67	11.21	15.31	34.08

This is mainly because the average heat exchange temperature difference in the heat exchanger HX3 is large. Specifically, the inlet temperature of the BDO mixture side is as high as 256.17 °C, and the inlet temperature of the bottom ORC fluid side using toluene is 126.90 °C. In addition, except for D4, the entropy generation of heat exchanger HX1 is the second largest. When D4 is used as the working fluid, the entropy generation of heat exchanger HX4 is significantly higher than that using other working fluids with a value of 15.01 %. When the bottom ORC fluid is toluene, benzene, cyclohexane, and D4, the entropy generation proportion of the bottom HP turbine is 13.84 %, 13.27 %,13.44 %, and 11.37 %, and it is 11.90 %, 12.73 %, 10.20 %, and 6.43 %, respectively for the LP turbine. The entropy generation of pumps *P*1, *P*2, and *P*3 is relatively low and not more than 1.18 %.

Table 11
Parameters of the CORC without any generators at different evaporation temperatures.

T_1 (°C)	T_4 (°C)	T_{10} (°C)	W_{top} (MW)	$W_{bot,HP}$ (MW)	$W_{bot,LP}$ (MW)	η_{top} (%)	$\eta_{bot,HP}$ (%)	$\eta_{bot,LP}$ (%)	$\eta_{CORC,max}$ (%)
360	228	125	3.59	2.89	3.52	12.67	11.78	16.36	35.30
365	233	127	3.53	2.92	3.55	12.53	11.92	16.58	35.46
370	238	130	3.48	2.91	3.61	12.41	11.94	16.89	35.62
375	243	132	3.43	2.94	3.63	12.28	12.06	17.09	35.76
380	248	135	3.38	2.93	3.69	12.15	12.06	17.39	35.90
385	253	137	3.34	2.95	3.72	12.03	12.16	17.59	36.03
390	258	139	3.29	2.96	3.75	11.90	12.25	17.78	36.16
395	263	142	3.25	2.95	3.80	11.78	12.23	18.06	36.27
400	268	144	3.20	2.97	3.83	11.66	12.31	18.25	36.38

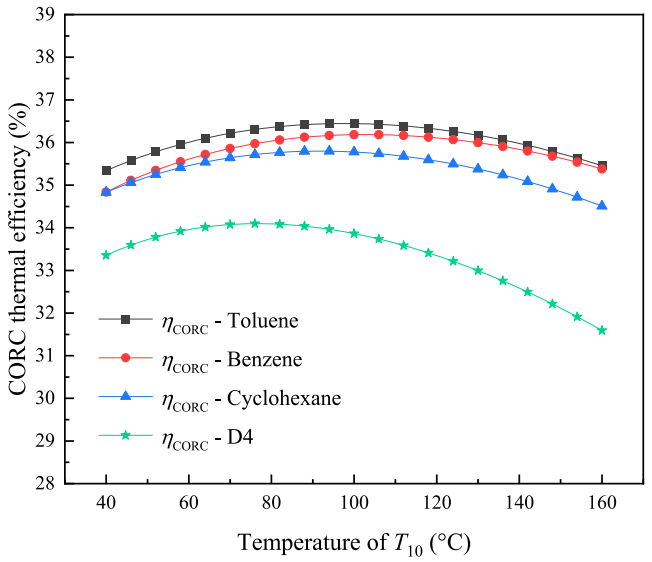

Fig. 20. Variation of the thermal efficiency of the CORC system without a top heat regenerator.

4.1.2. Influence of evaporation temperature

Section 4.1.1 focuses on the influence of the mixing chamber temperature and it is shown that as the bottom ORC fluid, toluene generally offers the highest efficiency. In this section, the effect of the evaporation temperature is investigated using toluene. The evaporation temperature of the top ORC system plays an important role in the performance of the system. An increased evaporation temperature can improve the heat-to-power conversation efficiency of the CORC system. The thermal efficiency of the CORC system in the evaporation temperatures range from 370 °C to 400 °C is shown in Fig. 8 and Fig. 9. The top ORC condensation temperature T_4 increases with the increment in T_1. The temperature difference between T_1 and T_4 is 132 °C to avoid a high pressure ratio of the top ORC turbine and a large degree of superheat after expansion. When the evaporation temperatures T_1 are 370 °C, 380 °C, 390 °C, and 400 °C, the CORC thermal efficiencies each are 39.18 %, 39.58 %, 39.94 %, and 40.26 %. The results show that the CORC thermal efficiency and the bottom HP ORC thermal efficiency increase continuously with the increase of evaporation temperature. When the evaporation temperature increases from 360 °C to 400 °C, the maximum CORC thermal efficiency relatively rises by 3.92 %.

The bottom ORC power output varying with the mixing chamber temperature at different evaporation temperatures is shown in Fig. 10. The variations are similar to those in Fig. 6 at 360 °C. As the evaporation temperature T_1 increases, the power output of the top ORC decreases since the condensation temperature of the top ORC increases, while the power output of the bottom HP ORC rises due to the increase in the inlet temperature of the bottom HP turbine. Detailed parameters at the maximum CORC thermal efficiency in the evaporation temperature range from 360 °C to 400 °C are given in Table 7. The optimum mixing chamber temperature increases with the increment in the top ORC evaporation temperature.

4.1.3. Influence of condensation temperature

The influence of the condensation temperatures on the performance of the high-temperature CORC system is also evaluated. In this section, the working fluid of the bottom ORC is still the toluene, and T_1 and T_4 are set to 360 °C and 228 °C. Variation of the thermal efficiency of the CORC system at different condensation temperatures is shown in Fig. 11. The condensation temperature is related to the ambient temperature. As the condensation temperature decreases, the CORC efficiency shows an increasing tendency. When T_{15} is 10 °C, 20 °C, 30 °C, and 40 °C, the maximum CORC thermal efficiency is 41.20 %, 39.97 %, 38.74 %, and 37.52 % at the mixing chamber temperature T_{10} of 84 °C, 91 °C, 98 °C, and 104 °C. The bottom HP ORC efficiency keeps constant at different condensation temperatures because it is determined only by the evaporation temperature (T_7) and the mixing chamber temperature (T_{10}) as shown in Fig. 12. However, the bottom LP ORC efficiency decreases with the increment in the condensation temperature (T_{15}).

Variation of the bottom ORC power output is shown in Fig. 13, and the detailed parameters at the maximum CORC thermal efficiency at the different condensation temperatures ranging from 10 °C to 40 °C are given in Table 8. As the condensation temperature increases, the power output of the bottom HP ORC and LP ORC increases and decreases, respectively. Meanwhile, the top ORC efficiency at maximum CORC efficiency remains the same while the optimum mixing chamber temperature increases.

4.2. Parametric analysis of the CORC without regenerators

Adding a regenerator to the basic ORC can recover part of the heat of the working fluid from the turbine, and at the same time reduce the heat load of the condenser and heat loss. The temperature of the working fluid at the inlet of the evaporator also goes up, thereby reducing the load of the evaporator. The performance of the CORC system with regenerators has been investigated in Section 4.1. To outline the thermodynamic advantage of the regenerators and make a comparison, the CORC performance without the regenerators is assessed in this section. There are two regenerators, one in the top ORC (HX2) and the other in the bottom ORC (HX4). The parametric analysis without any

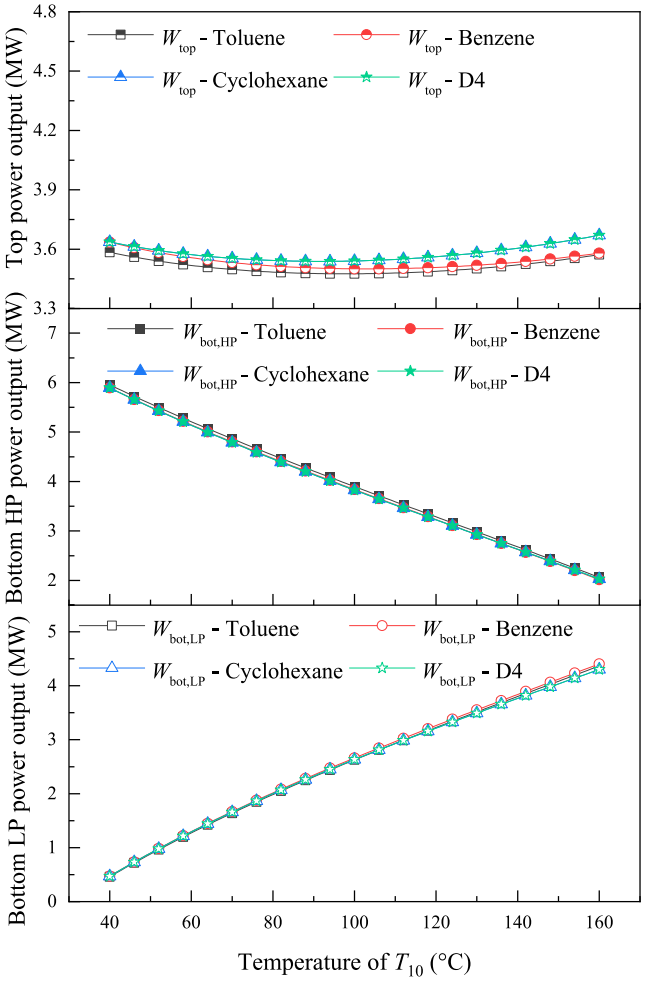

Fig. 21. Variation of the power output of the top, bottom HP, and bottom LP ORCs without a top regenerator.

Table 13
Parameters at the maximum CORC efficiency without a top regenerator.

	T_{10} (°C)	W_{top} (MW)	$W_{bot,HP}$ (MW)	$W_{bot,LP}$ (MW)	η_{top} (%)	$\eta_{bot,HP}$ (%)	$\eta_{bot,LP}$ (%)	$\eta_{CORC,max}$ (%)
Toluene	98	3.48	3.96	2.56	12.67	16.65	13.08	36.44
Benzene	103	3.50	3.75	2.75	12.67	15.64	13.77	36.19
Cyclohexane	92	3.54	4.07	2.39	12.67	16.83	11.99	35.80
D4	77	3.71	4.44	1.85	12.67	24.73	8.91	34.10

regenerator is implemented in Section 4.2.1. The scenarios without HX2 or HX4 are presented in Section 4.2.2 and 4.2.3.

4.2.1. CORC without any regenerators

Variation of the thermal efficiency of the CORC system without any regenerators is depicted in Fig. 14. HX2 and HX4 are excluded in the CORC system. The top ORC evaporation temperature and the bottom ORC condensation temperature are 360 °C and 30 °C. The total power output is still 10 MW. Compared with Fig. 3, the CORC efficiency without the two heat regenerators is obviously lower than that of the CORC system with HX2 and HX4. The maximum CORC thermal efficiency for the bottom ORCs using toluene, benzene, cyclohexane, and D4 is 35.30 %, 35.37 %, 34.23 %, and 30.88 %, when the mixing chamber temperature T_{10} is 125 °C, 123 °C, 124 °C, and 119 °C, respectively. Variations of the bottom ORC thermal efficiency without any heat regenerators are given in Fig. 15. When the mixing chamber temperature is 40 °C, 80 °C, 120 °C, and 160 °C, the bottom HP ORC thermal efficiency using toluene is 23.85 %, 16.98 %, 12.35 %, and 7.75 %, and the bottom LP ORC thermal efficiency is 2.53 %, 10.41 %, 15.81 %, and 19.61 %, respectively.

Variations of the power outputs of the top, bottom HP, and bottom LP ORCs without any regenerators are shown in Fig. 16. Compared with the CORC system with HX2 and HX4 (Fig. 6), the power output of the top ORC is decreased, indicating that the regenerator has a more significant impact on the top ORC than on the bottom one. When the working fluids are toluene, benzene, cyclohexane, and D4, the minimum power output of the top ORC without the regenerators is 3.59 MW, 3.58 MW, 3.70 MW, and 4.10 MW. Taking toluene as an example, when T_{10} is 40 °C, 80 °C, 120 °C, and 160 °C, the power output of bottom HP ORC is 5.70 MW, 4.23 MW, 3.03 MW, and 1.92 MW, and it is 0.51 MW, 2.13 MW, 3.38 MW, and 4.46 MW, respectively for the bottom LP ORC. The detailed parameters at the maximum CORC thermal efficiency of different working fluids are given in Table 9. Compare with the results in Table 5, due to the increased mixing chamber temperature at the maximum CORC thermal efficiency, the bottom HP ORC thermal efficiency decreases, while the bottom LP ORC thermal efficiency rises. The parameter distribution at maximum CORC efficiency of the high-temperature CORC system without any regenerators which uses toluene as the bottom ORC fluid is also given in Table 10.

The entropy generation of the high-temperature CORC system without heat regenerators at the maximum CORC efficiency is shown in Fig. 17. The entropy generations of the heat exchangers HX1, HX3, and mixing chamber are in the top three proportions, and the sum of them is about 56.84 %~72.69 % of the total entropy generation of the CORC system. The absence of HX2 and HX4 results in a significant increase in the entropy generation of HX1 and mixing chamber, which is particularly evident for the system using D4. For this reason, the CORC thermal efficiency of the system using D4 drops the most.

The thermal efficiency of the CORC system using toluene as the working fluid of the bottom ORC at the evaporation temperatures range

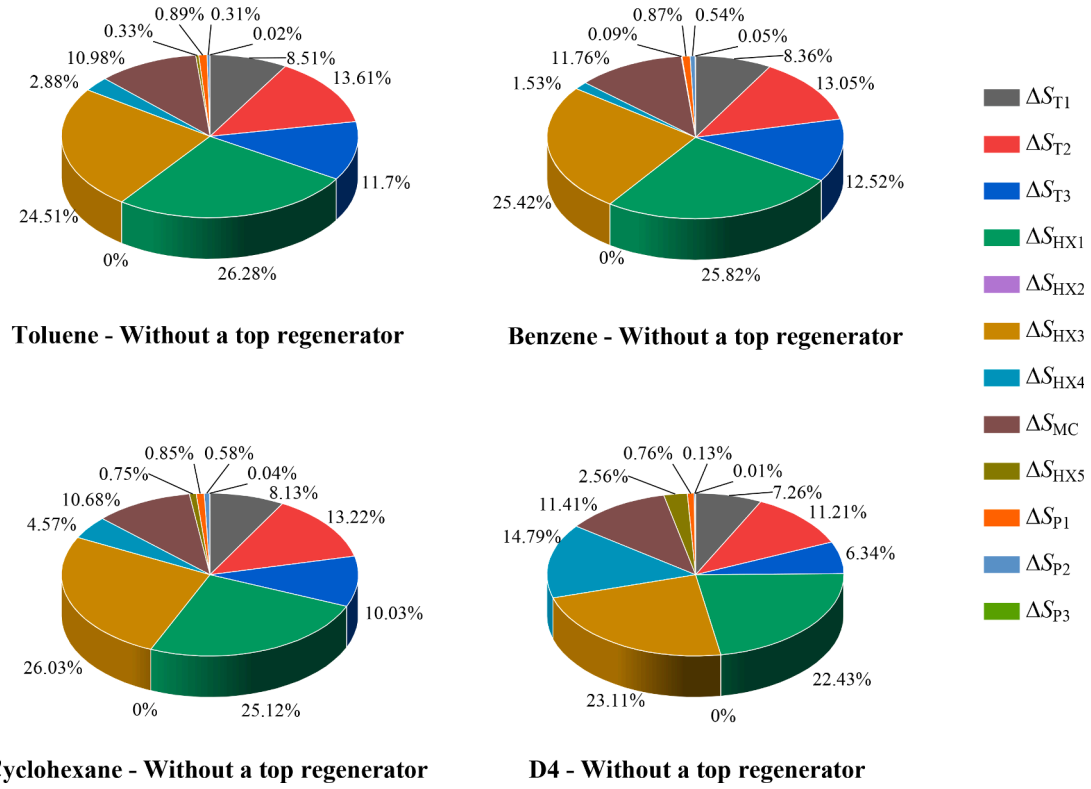

Fig. 22. Entropy generation at maximum CORC efficiency without a top heat regenerator.

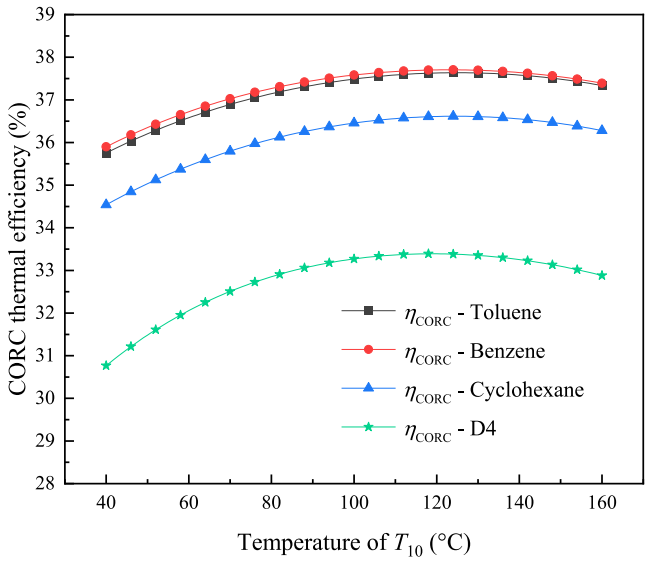

Fig. 23. Variation of the thermal efficiency of the CORC system without a bottom regenerator.

from 370 °C to 400 °C is shown in Fig. 18. When the evaporation temperature T_1 is 370 °C, 380 °C, 390 °C, and 400 °C, the CORC thermal efficiency is 35.62 %, 35.90 %, 36.16 %, and 36.38 %, respectively. The detailed parameters of the CORC system without heat regenerators at the maximum CORC thermal efficiency at different evaporation temperatures are given in Table 11. The CORC thermal efficiency increases continuously with the increase of evaporation temperature. When evaporation temperature rises from 360 °C to 400 °C, the maximum CORC thermal efficiency relatively increases by 3.07 %. This increment is less appreciable than that when the CORC system uses HX2 and HX4.

Variation of the thermal efficiency of the CORC system without any regenerators under different condensation temperatures is shown in Fig. 19. When the condensation temperature is 10 °C, 20 °C, 30 °C, and 40 °C, the maximum CORC thermal efficiency is 38.75 %, 36.52 %, 35.30 %, and 34.08 % at the mixing chamber temperature of 115 °C, 120 °C, 125 °C, and 130 °C, respectively. The mixing chamber temperature T_{10} at the maximum CORC thermal efficiency is higher than that in Table 8 with HX2 and HX4. The optimum T_{10} is a compromise among the efficiencies of the top ORC, bottom HP ORC, and bottom LP ORC. A higher T_{10} leads to a higher efficiency of the bottom LP ORC but a lower efficiency of the HP ORC. The bottom HP ORC and top ORC are less efficient without the regenerators and the LP ORC efficiency becomes more influential. Therefore, the optimum T_{10} is higher than that of the system with regenerators to increase the impact of the bottom LP ORC and the overall CORC efficiency. The detailed parameters of the CORC system without heat regenerators at the maximum CORC thermal efficiency at the different condensation temperatures are given in Table 12.

4.2.2. CORC without a top regenerator

Variation of the thermal efficiency of the CORC system without a top heat regenerator (HX2) is displayed in Fig. 20. The maximum CORC thermal efficiency for the bottom ORCs using toluene, benzene, cyclohexane, and D4 is 36.44 %, 36.19 %, 35.80 %, and 34.10 %, which is relatively reduced by 5.92 %, 5.99 %, 6.09 %, and 6.54 % compared to that with HX2. Since the evaporation temperature of the bottom HP ORC and the condensation temperature of the bottom LP ORC remain the same, the thermal efficiencies of the bottom ORCs are unchanged. Variations of the power outputs of the top, bottom HP, and LP ORCs without the top heat regenerator are displayed in Fig. 21. It can be seen that the power output of the top ORC is obviously reduced compared with the CORC system with HX2. When the working fluid of the bottom ORCs is toluene, benzene, cyclohexane, and D4, the minimum power output of the top ORC without a top regenerator is 3.48 MW, 3.50 MW, 3.54 MW, and 3.71 MW. The optimum mixing chamber temperature, power output, and thermal efficiency of the top, bottom HP, and bottom LP ORCs at the maximum CORC thermal efficiency are also presented in Table 13. The top ORC thermal efficiency is only 12.67 %, which is lower than that of the CORC system with heat exchanger HX2 (15.89 %), and this is the main reason for the decrease in the CORC thermal efficiency.

The entropy generation of the high-temperature CORC system without a top heat regenerator at the maximum CORC efficiency is shown in Fig. 22. The entropy generation of the heat exchanger HX3 and HX1 are still in the top two places, and the sum of the two is about half of the total entropy generation of the CORC system. Compared with the system in Section 4.1, the entropy generation of turbines T1, T2, and, T3 is reduced, and the values are around 7.26 % ~ 8.52 %, 11.21 % ~ 13.61 %, and 6.34 % ~ 12.52 %, respectively. The entropy generation of pumps *P*1, *P*2, and *P*3 is lower than 0.89 %.

4.2.3. CORC without a bottom regenerator

The regenerator (HX4) in the bottom HP ORC also has effects on the performance of the CORC system. As shown in Fig. 23, the maximum CORC thermal efficiency using toluene, benzene, cyclohexane, and D4 is 37.64 %, 37.70 %, 36.62 %, and 33.39 % when the mixing chamber temperature T_{10} is 125 °C, 123 °C, 124 °C, and 119 °C, respectively. Compared with the CORC system with HX4, the maximum CORC thermal efficiency is relatively reduced by 2.85 %, 2.04 %,3.94 %, and 8.48

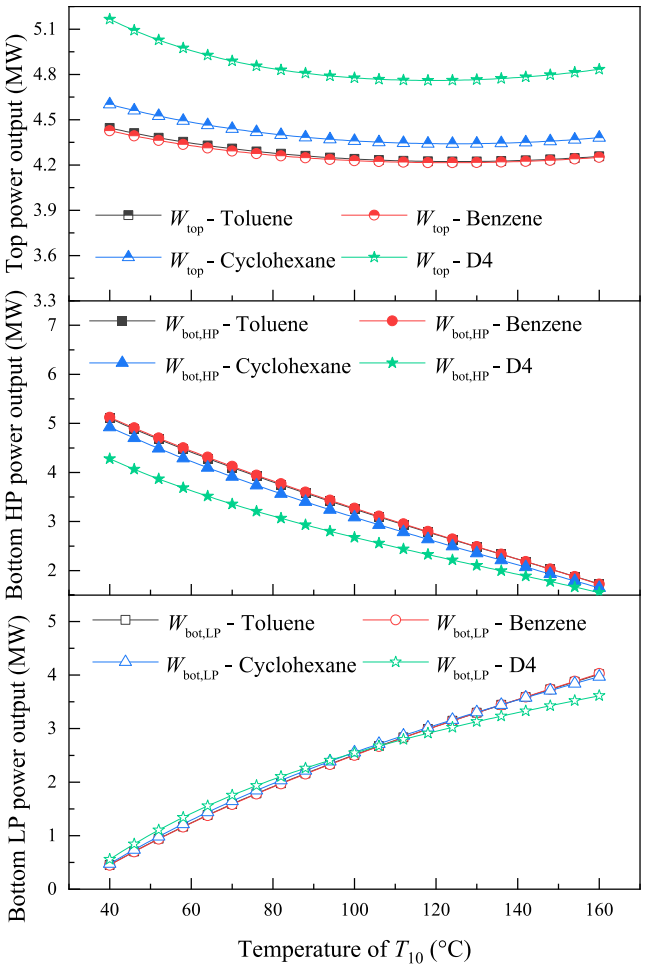

Fig. 24. Variation of the power output of the top, bottom HP, and bottom LP ORCs without a bottom regenerator.

Table 14
Parameters at the maximum CORC efficiency without a bottom regenerator.

	T_{10} (°C)	W_{top} (MW)	$W_{bot,HP}$ (MW)	$W_{bot,LP}$ (MW)	η_{top} (%)	$\eta_{bot,HP}$ (%)	$\eta_{bot,LP}$ (%)	$\eta_{CORC,max}$ (%)
Toluene	125	4.22	2.61	3.17	15.89	11.78	16.36	37.64
Benzene	123	4.21	2.67	3.12	15.89	12.08	16.18	37.70
Cyclohexane	124	4.34	2.49	3.17	15.89	10.97	15.74	36.62
D4	119	4.76	2.31	2.93	15.89	9.25	13.03	33.39

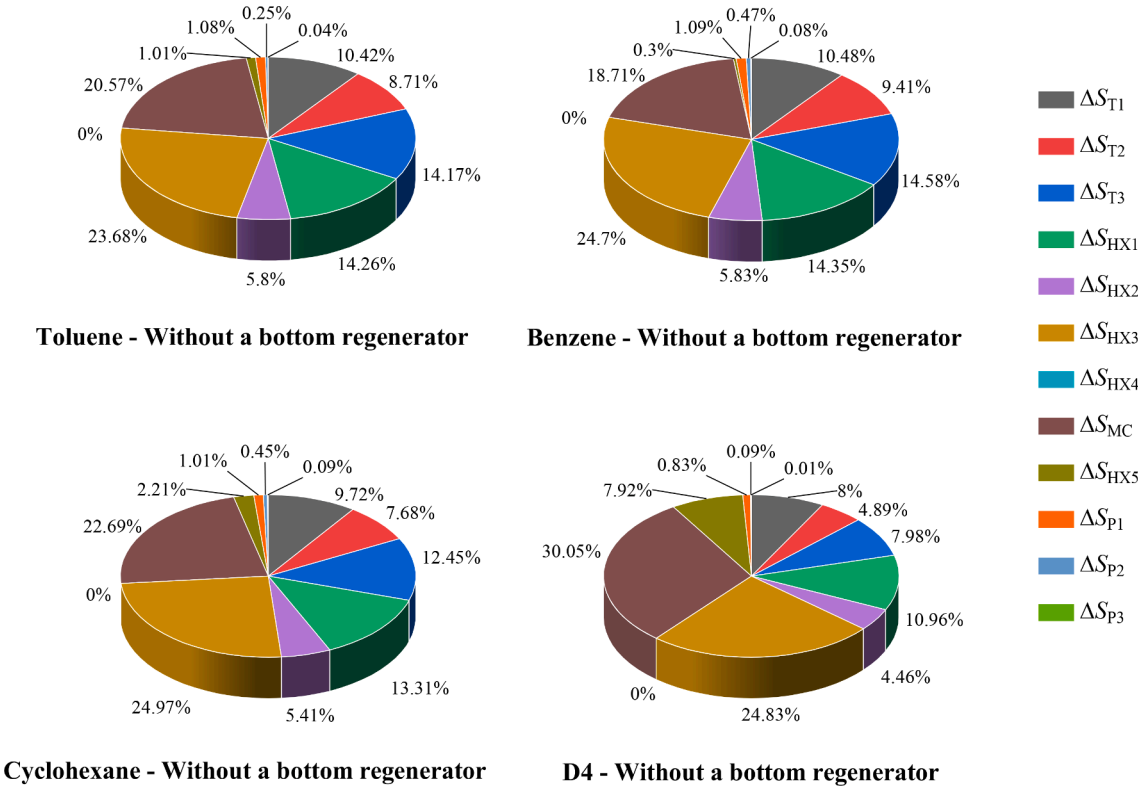

Fig. 25. Entropy generation at maximum CORC efficiency without a bottom regenerator.

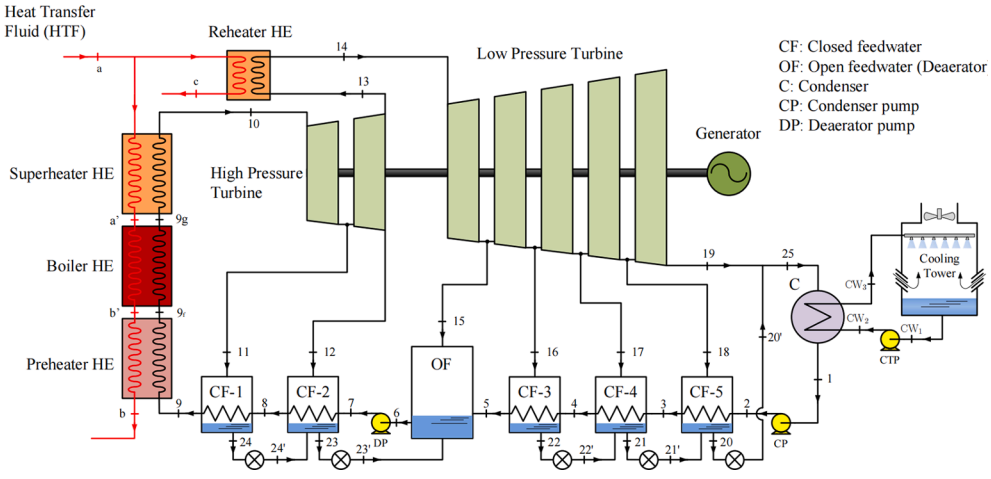

Fig. 26. The referenced SRC system [45].

%. Among them, HX4 has the most obvious effect on the system performance with D4 as the bottom ORC working fluid. For the other three working fluids, the influence of HX4 on the performance of the CORC system is less significant than that of HX2. Since the evaporation temperature of the bottom HP ORC and the condensation temperature of the bottom LP ORC remain the same, the thermal efficiencies of the bottom ORCs are the same to those in Fig. 15.

Variation of the power output of the top and bottom ORCs without HX4 is shown in Fig. 24. Compared with the CORC system with HX4, the power output of the top ORC is elevated, while the value of the bottom

Table 15
Economic assessment of the high temperature CORC system.

Equipment	W (kW)	A (m^2)	Cost (thousand $)
Top turbine	4441.01		2144.8
Bottom turbine	6215.04		2713.7
Generator	10123.25		383.0
*P*1	50.42		55.3
*P*2	69.02		49.3
*P*3	3.81		15.3
HX1		952.8	346.2
HX2		2045.8	488.6
HX3		3696.9	684.1
HX4		1100.5	237.5
HX5		1994.2	465.2
CORC			**7583.0**

HP ORC is reduced. When the working fluids are toluene, benzene, cyclohexane, and D4, the minimum power output of the top ORC without HX4 is 4.22 MW, 4.21 MW, 4.34 MW, and 4.76 MW. Taking toluene as an example, when T_{10} is 40 °C, 80 °C, 120 °C, and 160 °C, the power output of the bottom HP ORC is 5.10 MW, 3.80 MW, 2.73 MW, and 1.73 MW, and for the bottom LP ORC, it is 0.45 MW, 1.91 MW, 3.04 MW, and 4.01 MW, respectively. Table 14 provides the detailed parameters at the maximum CORC thermal efficiency of different working fluids. Compare with the results in Table 5, due to the increased mixing chamber temperature at the maximum CORC thermal efficiency, the bottom HP ORC thermal efficiency decreases, but the bottom LP ORC thermal efficiency rises.

The entropy generation of the CORC system without the bottom regenerator at the maximum CORC efficiency is shown in Fig. 25. Except for D4, the entropy generation of heat exchanger HX3 still accounts for the largest amount of the total entropy generation of the CORC system. It can be clearly seen that the lack of heat exchanger HX4 leads to a significant increase in the entropy generation of mixing chamber, and the increment is particularly obvious for the system using D4.

Table 16
Economic assessment of the conventional SRC system.

Equipment	W (kW)	A (m^2)	Cost (thousand $)
HP turbine	2958.21		1613.9
LP turbine	7720.49		3158.7
Generator	10144.77		383.8
CP	10.50		24.4
DP	13.43		42.7
Reheater		174.5	121.9
Superheater		230.3	226.5
Boiler		1526.9	789.8
Preheater		430.5	302.9
Condenser		643.3	197.0
CF-1		684.3	400.3
CF-2		304.9	198.9
CF-3		204.8	78.5
CF-4		138.8	49.6
CF-5		158.9	53.5
SRC			**7642.4**

4.3. Economic assessment

In this section, the economic performance of the high temperature CORC system with regenerators is compared with that of a conventional SRC system [45,46], as shown in Fig. 26. Thermal oil is the heat transfer fluid of the heat source for both systems, while water is the cooling medium. The temperatures of the thermal oil from the heat source and cooling water of the condenser are 400 °C and 20 °C, respectively. The rated net outputs of the CORC and SRC systems are both 10 MW_e. The CORC system works at $T_1 = 360$ °C and $T_{15} = 35$ °C with toluene as bottom ORC fluid and its heat-to-power conversion efficiency is 38.13 %. The reference SRC system operates at $T_{10} = 370$ °C, $T_{9g} = 300$ °C and $P_{10} = 9$ MPa, and has higher efficiencies for the major components than the CORC, e.g., an HP turbine efficiency of 85.5 %, an LP turbine efficiency of 89.5 % and a generator efficiency of 98 %. Its thermal efficiency is 38.21 % at nominal conditions [46]. The thermal efficiencies of the two systems are similar. Notably, the efficiency of the CORC will be higher if the generator efficiency is elevated from 95 % as listed in Table 4 to 98%.

The capital costs of the CORC and SRC systems are listed in Table 15 and Table 16. The total investment costs of the CORC and SRC system are 7583.0 thousand US dollars ($) and 7642.4 thousand $. For both systems, turbines cost the most. The costs of top and bottom turbines (4858.5 k $) account for about 64.07 % of the total CORC cost, while this ratio is 62.45 % (4772.6/7642.4) for the SRC. The cost difference between ORC turbines and steam turbines is minor because it is calculated by the same cost model with a total output of 10 MW. In practice, the ORC turbines may have lower capital and maintenance costs, because they have lower technical requirements than wet steam turbines that suffer from intense erosion by the droplets during the expansion process. The costs of the heat exchangers are the second highest. Shell and tube heat exchangers are used in the CORC and SRC systems, which have the advantages of high operating pressure/temperature, high heat transfer value, and low costs [47]. In the CORC system, the maximum heat transfer area is for HX3 (3696.9 m^2), and the maximum area in the SRC system is for the boiler (1526.9 m^2). The total surface area of the heat exchangers in the CORC is larger than that in the SRC. However, water preheater, boiler, superheater, etc., in the SRC have a higher operation pressure (9 MPa) than the heat exchangers (<1.1 MPa) in the CORC, thereby contributing to a higher pressure factor in the cost equation (Eq.44). The pump costs are lowest among the components in both two systems.

In the above comparison, because the reference solar SRC system uses thermal oil as the heat transfer fluid, the evaporation temperature of the BDO mixture in the CORC system is 360 °C but not 400 °C to allow

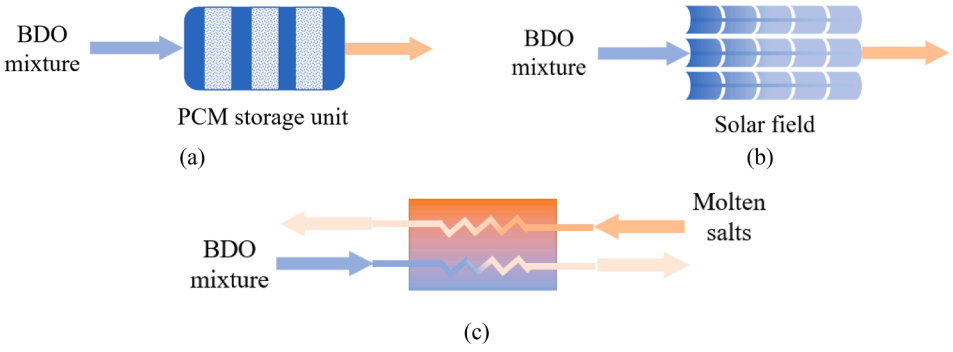

Fig. 27. Potential application of the high-temperature CORC.

a moderate cost of the HX1 and an acceptable temperature difference between heat transfer fluid and power fluid. Thermal oil is just a type of heat transfer fluid. Notably, the proposed CORC can also use phase change materials (PCMs), solar collectors, and molten salts as the heat sources, and has potential applications for heat battery and concentrated solar power generation, as shown in Fig. 27. Heat batteries, also known as Carnot batteries, have the advantage of high specific energy when using PCM storage. Some prototypes have been built [48]. The isothermal evaporation and condensation of the Rankine cycle make a good match with the PCM storage units. Compared with a conventional SRC, the CORC has a higher evaporation temperature of about 400 °C with a higher efficiency. It can be more cost-effective. In the concentrated solar power application, the BDO mixture may evaporate directly in the solar field as illustrated by Fig. 27 (b), and eliminate the HX1. Therefore, the cost of the power block will be further reduced. This is the ongoing research, and more results will be published in the near future.

5. Conclusions

In this paper, a parametric analysis of a high-temperature CORC system using BDO mixture as a top cycle fluid is carried out. An ORC efficiency model based on the equivalent hot side temperature is built, and the in-depth performance prediction and parametric analysis of the high-temperature CORC system are carried out. The results show that:

(1) Given a top ORC evaporation temperature of 360 °C and condensation temperature of 228 °C, the maximum CORC thermal efficiency using toluene, benzene, cyclohexane, and D4 as a bottom cycle fluid is 38.74 %, 38.49 %, 38.12 % and 36.48 % with the mixing chamber temperature of 98 °C, 103 °C, 92 °C, and 77 °C. The higher the mixing chamber temperature, the lower the bottom HP ORC thermal efficiency and the higher the bottom LP ORC thermal efficiency.
(2) An increased evaporation temperature and decreased condensation temperature can improve the heat-to-power conversation efficiency of the CORC system. When the evaporation temperature is 370 °C, 380 °C, 390 °C, and 400 °C, the maximum CORC thermal efficiency reaches 39.18 %, 39.58 %, 39.94 %, and 40.26 %. When condensation temperature is 10 °C, 20 °C, 30 °C, and 40 °C, the optimal CORC thermal efficiency is 41.20 %, 39.97 %, 38.74 %, and 37.52 %, respectively. The efficiency promotion of the CORC system at high temperatures is large. Notably, an efficiency of about 40 % is comparable or even higher than that of a conventional concentrated solar power system using parabolic trough collectors. The proposed CORC is thus potentially applicable in the solar power generation application.
(3) The regenerators have a significant impact on the CORC performance, probably because the BDO mixture, toluene, benzene, cyclohexane, and D4 are dry fluids. The fluids overcome the challenges of wet steam turbines and benefit from heat recovery from the regenerators. Without the regenerators, the maximum CORC thermal efficiency using the above fluids drops by 5 % −7%. The regenerator in the top ORC has a greater impact on thermal performance than the bottom regenerator.
(4) The proposed CORC system has a similar cost to a conventional SRC system at a given power output of 10 MW. The total capacity costs are 7583.0 k $ and 7642.4 k $, respectively. The predominant costs are for turbines. The CORC is expected to have a lower maintenance cost due to the elimination of wet steam turbines and can be more cost-effective when applied in heat batteries with PCMs and direct vapor generation solar thermal power systems.

CRediT authorship contribution statement

Xiao Ren: Data curation, Formal analysis, Investigation, Software. **Jing Li:** Conceptualization, Methodology, Formal analysis, Resources. **Gang Pei:** Supervision, Resources. **Pengcheng Li:** Data curation, Software. **Liang Gong:** Resources.

Declaration of Competing Interest

The authors declare that they have no known competing financial interests or personal relationships that could have appeared to influence the work reported in this paper.

Data availability

Data will be made available on request.

Acknowledgments

The study was sponsored by National Natural Science Foundation of China (52206292), China Postdoctoral Science Foundation (2022M713463), and the EU Marie Curie International Incoming Fellowships Program (703746).

Appendix A

The single-phase heat transfer area of the heat exchangers is expressed as:

$$A_{HX} = \frac{Q}{U\Delta T_m} \tag{A1}$$

where Q is the heat duty of the heat exchanger; U and ΔT_m are the overall heat transfer coefficient (W/(m^2·K)) and the log-mean temperature difference (K), and written as:

$$\frac{1}{U} = \frac{1}{\alpha_{tube}} + \frac{\delta}{\lambda} + \frac{1}{\alpha_{shell}} \tag{A2}$$

$$\Delta T_m = (\Delta T_{max} - \Delta T_{min}) \Big/ \ln\left(\frac{\Delta T_{max}}{\Delta T_{min}}\right) \tag{A3}$$

where δ and λ are the thickness (m) and the thermal conductivity of the tube wall (W/(m·K)); ΔT_m are the maximum and minimum temperature difference of the inlet and outlet (K); α is the convection heat transfer coefficient of the fluid in the tube side and shell side (W/(m^2·K)) [49], and calculated by:

$$\alpha_{\text{tube}} = \frac{\lambda}{D_{\text{tube}}}\left(\frac{\frac{f}{8}\cdot Re\cdot Pr}{12.7\left(\frac{f}{8}\right)^{0.5}\left(Pr^{\frac{2}{3}}-1\right)+1.07}\right) \tag{A4}$$

$$\alpha_{\text{shell}} = 0.36\left(\frac{\lambda}{D_{\text{shell}}}\right)\left(\frac{D_{\text{shell}}u}{\nu}\right)^{0.55} Pr^{\frac{1}{3}}\left(\frac{\nu}{\nu_{\text{tube}}}\right)^{0.14} \tag{A5}$$

where D_{tube} and D_{shell} are the diameter of the tube and shell (m); u is flow velocity (m/s); ν is the kinematic viscosity (m^2/s); f is the Darcy resistance coefficient, and expressed as

$$f = \frac{1}{(1.82\lg Re - 1.64)^2} \tag{A6}$$

For the evaporation and condensation process[50,51], the coefficients in the binary phase region are given as:

$$U_{\text{eva}} = 0.023\left[\frac{G(1-x)D}{\rho\cdot\nu}\right]^{0.8} Pr^{0.4}\frac{\lambda}{D}\left[1+3000\text{Bo}^{0.86}+1.12\left(\frac{x}{1-x}\right)^{0.75}\left(\frac{\rho_l}{\rho_v}\right)^{0.41}\right] \tag{A7}$$

$$U_{\text{con}} = 0.023\left[\frac{G(1-x)D}{\rho\cdot\nu}\right]^{0.8} Pr^{0.4}\frac{\lambda}{D}\left[(1-x)^{0.8}+\frac{3.8x^{0.76}(1-x)^{0.04}}{Pr^{0.38}}\right] \tag{A8}$$

where G is the mass flux ($kg/(m^2/s)$); Bo is the boiling number; ρ_l and ρ_v are the density of the liquid and vapor (kg/m^3); x is the liquid of working fluid.

References

[1] Anurag Kumar DR. A critical review on waste heat recovery utilization with special focus on Organic Rankine Cycle applications. Clean Eng Technol 2021;5:100292.
[2] Bellos E, Tzivanidis C. Investigation of a hybrid ORC driven by waste heat and solar energy. Energ Conver Manage 2018;156:427–39.
[3] Yang Y, Huo YW, Xia WK, Wang XR, Zhao P, Dai YP. Construction and preliminary test of a geothermal ORC system using geothermal resource from abandoned oil wells in the Huabei oilfield of China. Energy 2017;140:633–45.
[4] Roumpedakis TC, Loumpardis G, Monokrousou E, Braimakis K, Charalampidis A, Karellas S. Exergetic and economic analysis of a solar driven small scale ORC. Renew Energy 2020;157:1008–24.
[5] Karellas S, Braimakis K. Energy-exergy analysis and economic investigation of a cogeneration and trigeneration ORC-VCC hybrid system utilizing biomass fuel and solar power. Energ Conver Manage 2016;107:103–13.
[6] Wang M, Jing R, Zhang HR, Meng C, Li N, Zhao YR. An innovative Organic Rankine Cycle (ORC) based Ocean Thermal Energy Conversion (OTEC) system with performance simulation and multi-objective optimization. Appl Therm Eng 2018;145:743–54.
[7] Chen T, Zhuge WL, Zhang YJ, Zhang L. A novel cascade organic Rankine cycle (ORC) system for waste heat recovery of truck diesel engines. Energ Conver Manage 2017;138:210–23.
[8] Gao GT, Li J, Li PC, Cao JY, Pei G, Dabwan YN, et al. Design of steam condensation temperature for an innovative solar thermal power generation system using cascade Rankine cycle and two-stage accumulators. Energ Conver Manage 2019;184:389–401.
[9] Vescovo R, Spagnoli E. High Temperature ORC Systems. 4th International Seminar on Orc Power Systems. 2017;129:82-9.
[10] Shu GQ, Yu GP, Tian H, Wei HQ, Liang XY, Huang ZY. Multi-approach evaluations of a cascade-Organic Rankine Cycle (C-ORC) system driven by diesel engine waste heat: Part A - Thermodynamic evaluations. Energ Conver Manage 2016;108:579–95.
[11] Wang EH, Yu ZB, Zhang HG, Yang FB. A regenerative supercritical-subcritical dual-loop organic Rankine cycle system for energy recovery from the waste heat of internal combustion engines. Appl Energy 2017;190:574–90.
[12] Sanaye S, Khakpaay N. Thermo-economic multi-objective optimization of an innovative cascaded organic Rankine cycle heat recovery and power generation system integrated with gas engine and ice thermal energy storage. J Energy Storage 2020;32:101697.
[13] Weitzer M, Mueller D, Steger D, Charalampidis A, Karellas S, Karl J. Organic flash cycles in Rankine-based Carnot batteries with large storage temperature spreads. Energ Conver Manage 2022;255:115323.
[14] Kumar A, Shukla SK. Analysis and performance of ORC based solar thermal power plant using benzene as a working fluid. Proc Tech 2016;23:454–63.
[15] Abdullah MY, Prabowo P, Sudarmanta B. Efficiency analysis of refrigerant work fluid in the Organic Rankine Cycle (ORC) as an energy generating machine electricity 1 kW scale. 4th Annual Applied Science and Engineering Conference 2019.
[16] Gao GT, Li J, Li PC, Yang HL, Pei G, Ji J. Design and analysis of an innovative concentrated solar power system using cascade organic Rankine cycle and two-tank water/steam storage. Energ Conver Manage 2021;237:114108.
[17] Zhang YF, Li MJ, Ren X, Duan XY, Wu CJ, Xi H, et al. Effect of heat source supplies on system behaviors of ORCs with different capacities: An experimental comparison between the 3 kW and 10 kW unit. Energy 2022;254:124267.
[18] Jankowski M, Borsukiewicz A. Multi-objective approach for determination of optimal operating parameters in low-temperature ORC power plant. Energ Conver Manage 2019;200.
[19] Moens L, Blake DM. Mechanism of hydrogen formation in solar parabolic trough receivers. J Sol Energ-T Asme 2010;132:031006.
[20] Vishwakarma S, Debnath BK, Debnath K, Das B. Comparative Analysis of Absorber Tubes of Parabolic Trough Solar Collector Using Therminol VP-1 as Heat Transfer Fluid. Lect N. Mech Eng 2020:1227–40.
[21] Mwesigye A, Yilmaz IH, Meyer JP. Numerical analysis of the thermal and thermodynamic performance of a parabolic trough solar collector using SWCNTs-Therminol (R) VP-1 nanofluid. Renew Energy 2018;119:844–62.
[22] Habibi H, Zoghi M, Chitsaz A, Javaherdeh K, Ayazpour M. Thermo-economic performance comparison of two configurations of combined steam and organic Rankine cycle with steam Rankine cycle driven by Al2O3-therminol VP-1 based PTSC. Sol Energy 2019;180:116–32.
[23] Ju X, Abd El-Samie MM, Xu C, Yu HY, Pan XY, Yang YP. A fully coupled numerical simulation of a hybrid concentrated photovoltaic/thermal system that employs a therminol VP-1 based nanofluid as a spectral beam filter. Appl Energy 2020;264:114701.
[24] Niggemann RE. Organic Rankine Cycle Technology Program. https://www.osti.gov/biblio/47749291969.
[25] Bronicki LY. Ormat Rankine power unit. 7th intersociety energy conversion engineering conference. San Diego, California, USA1972.
[26] Anderson WG. Intermediate Temperature Fluids for Heat Pipes and Loop Heat Pipes. 5th International Energy Conversion Engineering Conference and Exhibit (IECEC). St. Louis, Missouri2007.
[27] Eastman. Therminol VP-1 Heat Transfer Fluid. https://www.therminol.com/product/710934592022.
[28] Egoï Ortego LV. Wet to dry cycles for high temperature waste heat valorisation using a diphenylbiphenyl oxide mixture. ORC2021 - 6th International Seminar on ORC Power Systems. Munich, Germany2021.
[29] Vescovo R. High Temperature Organic Rankine Cycle (HT-ORC) For Cogeneration of Steam and Power. Aip Conf Proc. 2019;2191.
[30] Eastman. Therminol ® VP-1 heat transfer fluid. 2021.
[31] Li J, Alvi JZ, Pei G, Su YH, Li PC, Gao GT, et al. Modelling of organic Rankine cycle efficiency with respect to the equivalent hot side temperature. Energy 2016;115:668–83.
[32] Wang X, Wang R, Jin M, Shu GQ, Tian H, Pan JY. Control of superheat of organic Rankine cycle under transient heat source based on deep reinforcement learning. Appl Energy 2020;278:115637.
[33] Kose O, Koc Y, Yagli H. Energy, exergy, economy and environmental (4E) analysis and optimization of single, dual and triple configurations of the power systems: Rankine Cycle/Kalina Cycle, driven by a gas turbine. Energ Conver Manage 2021;227:113604.
[34] Li PC, Cao Q, Li J, Lin HW, Wang YD, Gao GT, et al. An innovative approach to recovery of fluctuating industrial exhaust heat sources using cascade Rankine cycle and two-stage accumulators. Energy 2021;228:120587.
[35] Turton R, Bailie RC, Whiting WB, Shaeiwitz JA, Analysis BD. Synthesis, and Design of Chemical Processes. Pearson Education; 2012.

[36] Sohrabi A, Behbahaninia A, Sayadi S. Thermodynamic optimization and comparative economic analysis of four organic Rankine cycle configurations with a zeotropic mixture. Energ Conver Manage 2021;250:114872.
[37] Joshua Peacock GH, Song J, Markides CN. Techno-economic assessment of integrated spectral-beam-splitting photovoltaic-thermal (PV-T) and organic Rankine cycle (ORC) systems. Energ Conver Manage 2022;269:116071.
[38] Ren X, Li J, Gao GT, Pei G. An innovative concentrated solar power system driven by high-temperature cascade organic Rankine cycle. J Energy Storage 2022;52:104999.
[39] Thol M, Javed MA, Baumhogger E, Span R, Vrabec J. Thermodynamic Properties of Dodecamethylpentasiloxane, Tetradecamethylhexasiloxane, and Decannethylcyclopentasiloxane. Ind Eng Chem Res 2019;58:9617–35.
[40] Yu GP, Shu GQ, Tian H, Wei HQ, Liang XY. Multi-approach evaluations of a cascade-Organic Rankine Cycle (C-ORC) system driven by diesel engine waste heat: Part B-techno-economic evaluations. Energ Conver Manage 2016;108:596–608.
[41] Yagli H, Koc Y, Kalay H. Optimisation and exergy analysis of an organic Rankine cycle (ORC) used as a bottoming cycle in a cogeneration system producing steam and power. Sustain Energy Techn 2021;44:100985.
[42] Wilailak S, Yang JH, Heo CG, Kim KS, Bang SK, Seo IH, et al. Thermo-economic analysis of Phosphoric Acid Fuel-Cell (PAFC) integrated with Organic Ranking Cycle (ORC). Energy 2021;220:119744.
[43] Li TL, Meng N, Liu J, Zhu JL, Kong XF. Thermodynamic and economic evaluation of the organic Rankine cycle (ORC) and two-stage series organic Rankine cycle (TSORC) for flue gas heat recovery. Energ Conver Manage 2019;183:816–29.
[44] Song J, Gu CW. Parametric analysis of a dual loop Organic Rankine Cycle (ORC) system for engine waste heat recovery. Energ Conver Manage 2015;105:995–1005.
[45] Padilla RV. Simplified Methodology for Designing Parabolic Trough Solar Power Plants. University of South Florida; 2011.
[46] Montes MJ, Abanades A, Martinez-Val JM, Valdes M. Solar multiple optimization for a solar-only thermal power plant, using oil as heat transfer fluid in the parabolic trough collectors. Sol Energy 2009;83:2165–76.
[47] Li P, Lin H, Li J, Cao Q, Wang Y, Pei G, et al. Analysis of a direct vapor generation system using cascade steam organic Rankine cycle and two-tank oil storage. Energy 2022;257:124776.
[48] Dumont O, Frate GF, Pillai A, Lecompte S, De Paepe M, Lemort V. Carnot battery technology: A state-of-the-art review. J Energy Storage 2020;32:101756.
[49] Incropera FP, DeWitt DP. Fundamentals of heat and mass transfer. New York: John Wiley and Sons; 1996.
[50] Gungor KE, Winterton RHS. Simplified general correlation for saturated flow boiling and comparisons of correlations with data. Chem Eng Res Des 1987;65:148–56.
[51] Shah MM. A general correlation for heat transfer during film condensation inside pipes. Int J Heat Mass Transf 1979;22:547–56.